A SYSTEMATIC APPROACH TO CORRECT THE BANDGAP ERRORS IN DENSITY-FUNCTIONAL-THEORY BAND STRUCTURE CALCULATIONS FOR InV (V = P, As, Sb)

by

Premkumar Pugalenthi

A thesis submitted to the faculty of
The University of North Carolina at Charlotte
in partial fulfillment of the requirements
for the degree of Master of Science in
Mechanical Engineering

Charlotte

2012

Approved by:

_____
Dr. Yong Zhang

_____
Dr. Qiuming Wei

_____
Dr. Howie Fang

©2012
Premkumar Pugalenthi
ALL RIGHTS RESERVED

ABSTRACT

PREMKUMAR PUGALENTHI. A systematic approach to correct the bandgap errors in density-functional-theory band structure calculations for InV (V = P, As, Sb) (Under the direction of DR. YONG ZHANG)

Density Functional Theory (DFT) is a powerful tool for material design and understanding the material properties. DFT is often implemented in the so-called local density approximation (LDA). Although higher order theories are available, they are computationally too demanding for many real world problems, such as accurately predicting the electronic and optical properties of a new semiconductor nanostructure or heterostructure. In this work, we applied a new scheme to correct the electronic structures computed by DFT-LDA simultaneously for a set of binary semiconductors that can be used to generate various new structures for different applications such as Photovoltaics, Solid State Lighting. Specifically, we apply the method to a set of common cation binaries InV (V = P, As, Sb), and correct band gap errors of the DFT-LDA results to match very closely the experimental results, which lays the ground to predict the material properties of new structures involving these binaries.

ACKNOWLEDGMENT

First of all, I would like to express my heartfelt gratitude to my thesis advisor Dr. Yong Zhang for his meticulous and constant guidance and support throughout this work. As a renowned physicist in the field of solid state physics he always has been a role model in my life and taught me how to enjoy learning and doing research. I have been amazingly fortunate to work with him and I hope that one day I would become as good an advisor to my students as he has been to me.

I would like to thank my thesis committee members, Dr. Quiming Wei and Dr. Howie Fang for their sincere interest and constructive criticism, suggestion and advice for this work.

I would like to thank to Dr. Jianwei Wang, a talented postdoc in our group, for his support throughout the work on all the pseudopotential calculations.

I also would like to thank Dr. Lin-Wang Wang, Lawrence Berkeley National Laboratory for providing computational codes used in this work, and National Energy Research Scientific Computing Center (NERSC) for the use of its supercomputing facilities through the collaboration with Dr. Lin-Wang Wang.

I wish to express my sincere gratitude to all my friends for their friendship with consistent encouragement and love. Finally, and most importantly, I wish to thank my mother and father for their endless patience, support and love during all these years. Also, I would like to express my sincere gratitude to my sister. Without all their love and support, this thesis would not have been possible.

My humble pranams to AMMA for her blessings.

DEDICATION

I dedicate this to my Mother and Father

TABLE OF CONTENTS

LIST OF FIGURES

LIST OF TABLES

CHAPTER 1: INTRODUCTION

In this chapter we will present the motivation towards this research and the problem statement. We also present the importance of the theoretical method used in this thesis for the calculations of the electronic structure and the optical properties. We also give an overview of the distinctive electronic and optical properties of the InV (V=P, As, Sb) semiconductors, which led to this study.

1.1. Background

Energy demand of the world is estimated to increase more than double by 2050. Identifying a clean energy source for future is a tougher challenge for mankind since advances in existing energy system will not be sufficient in a sustainable way [1].

One of the clean energy source known to humans is the Sun. The amount of energy from the Sun in the form of sunlight striking the Earth per hour (4.3×10^{20} J) is more than energy used on the planet per year (4.1×10^{20} J) [1]. Presently, this solar resource is utilized as solar electricity because of photovoltaic conversion, first observed by the French scientist Edmund Becquerel in 1839 [2].

Solar cells contribute only less than 0.1% of the world total energy usage [3]. This stimulates the need for huge development in energy research to maximize the solar energy usage. Since, it is abundant, easily available, and no pollution problems as in fossil fuels.

Photovoltaic (PV) research covers mainly developing and improving PV cells in several material systems; developing advanced technologies; and improving performance and reliability. A major technological breakthrough in photovoltaic technology will be reduction in cost/watt of solar electricity produced. Recent trends in solar energy research are development of new materials which are energy efficient and new methods to sweep the full spectrum of wavelengths in solar radiation [4]. Additional design parameters can come from confinement effects which have led to intensified research on nanowires for photovoltaic applications [5]. Such developments in all aspects of solar technology will change the design, manufacturing and usage of solar cells in future.

1.2. Photovoltaic materials

From the beginning in mid 1950s, solar cells have an unbelievable growth, from Silicon PV devices to Nano Solar cells in present day. In early 1980s, III-V semiconductor devices, based on GaAs were used in PV cells, because of their improved efficiency compared to Si and better properties. Later, more complex heterostructures based on arsenides and phosphide multijunction solar cells were developed with an increased efficiency more than 20% [4]. In 2000, triple junction InGaP/GaAs/Ge device achieved the 30% efficiency. In last decade, III-V semiconductor devices replaced were widely used because of greater efficiency, low weight and better radiation resistance.

Very recently, in 2010, Nanophotovoltaics, the third generation PV, joins the quest to develop less-expensive solar panels that are cheaper to produce, and lighter than their predecessors. Scientists are conceiving and designing new photovoltaic panels using technologies including carbon nanotubes, multiple quantum wells, nanowires, nanoantennas, and quantum dots. The photovoltaic materials now used as bulk, when in

nano dimension are believed to exhibit far superior properties which will soon replace other PV technologies. Still, researchers are trying to find the optimum material to do the job of efficient energy conversion. Requirements for the ideal solar cell [6] material are

- Bandgap between 1.1 and 1.7 eV;
- Direct band structure;
- Consisting of readily available, non-toxic materials;
- Easy, reproducible deposition technique, suitable for large area production;
- Good photovoltaic conversion efficiency;
- Long-term stability.

The electronic band structures of these materials are among their most fundamental properties. Optical measurements and band-structure calculations are among the known techniques to understand the electronic band structures of these materials.

1.3. Band structure calculation techniques

The paper by Benjamin Lax [7], outlines the simultaneous efforts of theoretical studies by first principle band structure calculation and experimental studies of electrical and optical properties, which contributed to a better understanding of the band structure of solids. From the past, the theoretical studies lacked the ability to correctly predict the quantitative nature of bands. As in [7], experimental results have been used to modify and extend the theoretical calculations. Theoretical results were used to analyze experimental results. This symbiotic relationship helped us to elucidate many complex band structures from bulk germanium and silicon to ZnO/ZnSe nanowires.

The experimental techniques used for band structure elucidation are but not limited to de Haas-van Alphen effect, cyclotron resonance, galvano magnetic effect, and optical absorption [7]. The de Haas-van Alphen effect is a potent tool that provides quantitative and direct information on the curvature of bands at the Fermi surface in metals. The cyclotron resonance, a direct method provides additional information of the bands. Galvano magnetic measurements, such as Hall effort and magneto resistance were the oldest tools to elucidate bands in metals. Using optical absorption inter-band transitions can be studied.

Electronic band structure calculation methods can be categorized into two general groups [8]. The first one is empirical methods, such as the tight-binding [9] (also known as the Linear Combination of Atomic Orbitals (LCAO) method), the k.p method [10], and the local [11], or the non-local [12] empirical pseudopotential method (EPM). These methods involve empirical parameters to fit experimental data such as the band-to-band transitions at specific high-symmetry points derived from optical absorption experiments. The electronic structure can be calculated by solving a one-electron Schrödinger wave equation and hence computationally less expensive.

The continuum k· p effective-mass method has several limitations, especially for smaller systems. The tight-binding model is used successfully to simulate thousand-atom systems, yet the conduction band structure fitting is not accurate [13]. The empirical pseudopotential method (EPM) uses a sum of non-self-consistent screened pseudopotentials to represent the total potential of a system. EPM helps us to describe the electronic structure of nanosystems accurately by further improvisations such as fitting it to the ab initio bulk potentials; adding local environment-dependent pre-factors to

describe the deformation potentials; and rescaling the kinetic energy operator to mimic the effects of nonlocal potentials. The limitations of EPM include, for instance, non-self-consistent nature, and the difficult to find the corresponding surface passivation potentials [13].

The second one is ab initio methods, such as Hartree-Fock or Density Functional Theory (DFT), which calculate the electronic structure from first principles. Calculations with larger atoms (approximately 1000 atoms) are computationally expensive and require massively parallel computers [14]. Ab-initio methods such as the density functional theory (DFT) are more reliable than the EPM approach and can be used for almost any materials. The density functional theory (DFT) was formulated in the 60's of the past century by Hohenberg, Kohn and Sham [15] [16], that it has become the standard method in the calculation of the electronic structure of solids. One major disadvantage of this method is the large computational time required for thousand atom nanostructure calculations [17]. Density Functional Theory method with the local density approximation (LDA) calculation, band gap will be incorrect often. Therefore to overcome these limitations of DFT, a band-corrected pseudopotential scheme, which adds a small empirical correction to the ab-initio pseudopotential to reproduce the experimental bulk band gaps are used to elucidate the band structure of nanocrystals [18].

1.4. Problem statement

Electronic and optical properties of binary semiconductors are studied extensively, both experimentally and theoretically in past 20 years [11] [12]. Especially III-V semiconductors are extensively studied because of the prospect of obtaining unique electronic and optical properties by mixing different elements.

Nevertheless of interesting properties related to In-V (V=P, As, Sb) semiconductors narrow energy gaps [19], they have not been studied much [20] [21], in comparison to the extensive work performed on other III-V zinc-blende-structure materials like GaAs and AlAs. For In-V semiconductor nanowires, an extensive investigation of optical and electronic properties has not yet been performed. In order to facilitate this, as an initial step, we have performed an exhaustive band gap corrected first-principles calculations. In other words, a band-corrected pseudopotential scheme, which adds a small empirical correction to the ab-initio pseudopotential to reproduce the experimental bulk band gaps are used.

Band-structure calculations were performed using the PEtot code developed by L.W.Wang, which uses the ab-initio pseudopotential method within the LDA and neglects spin-orbit coupling. The original pseudopotentials are used in the self-consistent LDA calculations for the charge densities in fitting and following large system calculations, and the modified pseudopotentials are used in a post process to calculate the electronic structure of the system.

1.5. InV semiconductors

1.5.1. Indium phospide (InP)

InP (with a larger band gap of 1.42 eV) is considered as a promising material for nanowire-based applications. Some experimental studies of the band structure parameters for InP and its alloys have been carried out. Rochon and Fortin [22] found the low-temperature direct band gap to be 1.423eV. InP is a direct-gap semiconductor of great technological significance [23] [24] [25], since it serves as the substrate for most optoelectronic devices operating at the communications wave length of 1.55μm.

1.5.2. Indium arsenide (InAs)

InAs has assumed increasing importance in recent years as the electron quantum well material for InAs/GaSb/AlSb based electronics [26] and long-wave length optoelectronic [27] devices. The vast majority of experimental low-temperature energy gaps fall in the 0.41–0.42eV range [28] **,** although somewhat higher values have also been reported [29] [30]. The value 0.418 eV that was obtained from recent measurements on a high-purity InAs sample [31], is generally used.

1.5.3. Indium antimonide (InSb)

The InSb is the III–V binary semiconductor with the smallest band gap in infrared range is the staple material for infrared detector devices. For many years it has been a touchstone for band structure computational methods [32], partly because of the strong band mixing and nonparabolicity that result from the small gap. The primary technological importance of InSb arises from mid-infrared optoelectronics applications [33]**.**

CHAPTER 2: THEORY

In this chapter we outline the theoretical framework that underpins the bulk of this work. We begin with a summary of the bulk crystalline structure and electronic structure, and explain how the physics of condensed matter can be described by the many-electron Schrodinger equation. We describe the plane wave pseudopotential method, and also about the norm conserving pseudopotentials. We then discuss in more detail about the band gap corrected first-principles calculations based on the pseudopotential method.

2.1. General theory

Any theoretical model of semiconductor materials or devices starts from the one-electron energy level, *E* vs crystal wave vector, *k* relation. This band structure, which is constructed from the microscopic level, determines most of the macroscopic properties that are actually measured [34]. Computational solid state physics is modern area of research that encompasses mathematical techniques to calculate the electronic band structure. These techniques involve building of quite complicated mathematical model, to solve for the electronic band structure.

2.1.1. Crystal structure

InV (V= P, As, Sb) crystallizes under normal conditions in the zinc blende structure. It is customary to think of crystals as being build up out of simple building blocks called "unit cells." The primitive zinc blende structure (space group $F\bar{4}3m$) unit cell contains 2 atoms. There are several equivalent ways to define the unit cells. For the purpose of these initial calculations we will define the structures as follows:

The shape of the primitive 2-atom zinc blende cell is an equal-sided parallelepiped that can be most easily visualized with reference to a larger, 8-atom cubic cell as shown in figure 2.1.

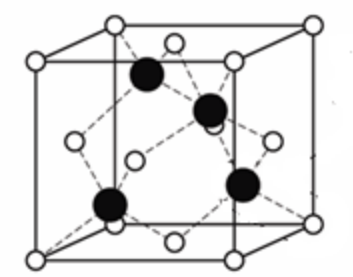

Figure 2.1 Zinc Blende Structure

This cubic cell has In-atoms at the origin and in the centre of each of the three faces that touch the origin. For each V (P, As, Sb)-atom, there is a In-atom at a displacement of $\left[\frac{1}{4},\frac{1}{4},\frac{1}{4}\right]$ away from it. The lattice vectors defining the primitive cell are the three vectors going from the origin to the centre of the three faces where the In-atoms are. These vectors are of equal length and are separated from each other by angles of 60^0. The three In-atoms on the faces of the cube are not in the primitive cell as they are simply the periodic repetitions of the atom at the origin. The primitive cell thus contains a V (P, As, Sb)-atom at [0,0,0] and a In-atom at $\left[\frac{1}{4},\frac{1}{4},\frac{1}{4}\right]$.

Kronig & Penney [34] developed a very simple one dimensional model that explains much of the motion of electrons through crystals. Three-dimensional Kronig & Penney quantum states can be formed as products of one-dimensional ones. For real three-di-mensional crystals, there are three periods, so called as “primitive translation

vectors" d_1, d_2, and d_3 and three dimensional wave number vector k with components k_x, k_y, and k_z.

In the Kronig & Penney model, the wave numbers could be reduced to a finite interval

$$-\frac{\pi}{d_x} \leq k_x < \frac{\pi}{d_x} \ , \tag{2.1}$$

This interval is called the first Brillouin zone. Wave numbers outside this zone are equivalent to ones inside. The general rule was that wave numbers a whole multiple of $\frac{2\pi}{d_x}$ apart are equivalent.

In three dimensions, the first Brillouin zone is no longer a one dimensional interval but a three dimensional volume. And the separations over which wave number vectors are equivalent are no longer so simple. Instead of simply taking an inverse of the period d_x, as in $\frac{2\pi}{d_x}$, matrix formed by the three primitive translation vectors d_1, d_2, and d_3 has to be inversed. Then, wave number vectors closest to the origin, which are enough to describe all quantum states are to be identified. Brillouin zone of zincblende structure is shown in figure 2.2.

Every single point in the first Brillouin zone corresponds to multiple Bloch waves, each with its own energy. To plot all those energies is not possible; it would require a four-dimensional plot. Instead, what is done is plot the energies along representative lines. Such plots will here be indicated as one dimensional energy bands. Note however that they are one dimensional band of true three dimensional crystals. They are not just Kronig & Penney model bands.

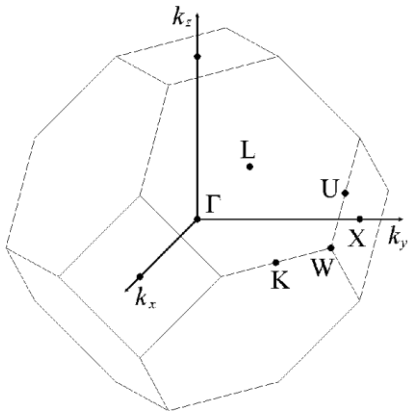

Figure 2.2 Brillouin zone of zincblende structure

Typical points between which one dimensional band is drawn are indicated in figure 2, named K, L, W, U, and X. The center of the Brillouin zone is the origin r, where the wave number vector is zero. These are the critical points in a Brillouin zone and the energies at this point, are very significant.

2.1.2. Electronic band structure

As said earlier, band structures is typically shown as a function of a one dimensional path through reciprocal space made up of straight lines connecting points of high symmetry. The electronic band structure of the material is the solution of the many body Schrodinger equation in the presence of the periodic potential of the lattice. The electronic solutions in the presence of the periodic potential [5] of the lattice are in the form of Bloch functions

$$\psi_{n,k} = u_n(k)e^{ik.r} , \qquad (2.2)$$

where k is the wave vector, and n labels the band index corresponding to different solutions for a given wave vector. The cell-periodic function, $u_n(k)$, has the periodicity of the lattice and modulates the traveling wave solution associated with free electrons.

A semiconductor can have a direct band gap or an indirect band gap. A direct band gap is characterized by having the band edges aligned in *k*, so that an electron can transit from the valence band to the conduction band, with the emission of a photon, without changing considerably the momentum. On the other hand, in the indirect band gap the band edges are not aligned so the electron does not transit directly to the conduction band. In this process both a photon and a phonon are involved. InAs band structure obtained with a non-local pseudopotential calculation [12] is shown in figure2.3. InV (V= P, As, Sb) are direct band gap semiconductors.

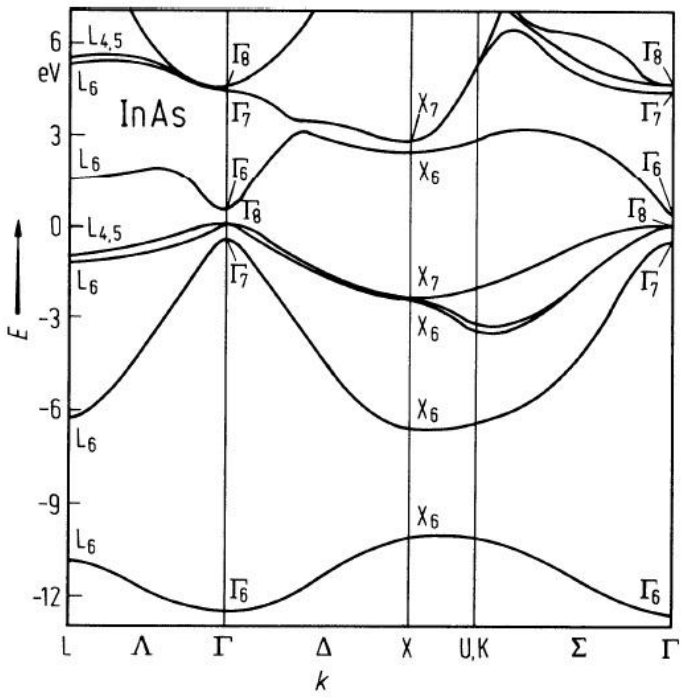

Figure 2.3 Band structure obtained with a non-local pseudopotential calculation [12]

The energetic levels in atoms and molecules can be discrete or can merge into a near-continuum of levels called a band. The energy bands can be classified as empty, filled, mixed or forbidden bands. The energetic levels are occupied by the electrons,

starting with the lowest energy value level. The electrons that contribute to the electrical conduction occupy the higher energy bands. The valence band corresponds to the highest energy band that contains electrons. The valence band can be fully or partial occupied. The allowed (empty) states in the valence band add contribution to the electric current. The conduction band is the lowest energetic band with unoccupied states for an insulator.

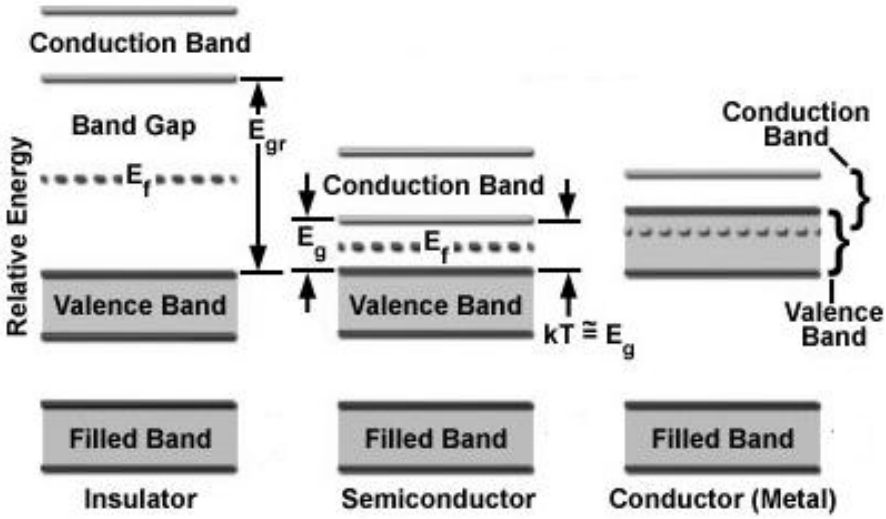

Figure 2.4 Energy band gaps in solids [35]

In materials the conducting bands of empty, filled or allowed states can interfere with forbidden bands, also called band gaps [35]. Also, the energy difference between the Valence Band Maximum (*VBM*) and the Conduction Band Minimum (CBM) is the band gap of the material. The width of the band gap (width measured in energy units) determines the type of material: insulator, semiconductor, metal as shown in figure [35].

The band structure of a semiconductor is of pivotal importance in the understanding the properties of the material in response to applied fields and to determine

its potential applications. Most of the fundamental optical properties, such as the optical absorption or the photoluminescence, are basically determined by the features of the bands adjacent to the band gap, often near the r point. The proper description of this region is therefore of crucial importance for realistic predictions about the optical properties of the semiconductors.

2.2. Density functional theory

Many of the physical properties of solids are related to total energies or to total energy differences. For instance, the equilibrium lattice constant of a crystal is given by the atomic spacing that minimizes the total energy. Surfaces and defects of solids adopt the structure that minimizes their corresponding total energies. If total energies can be calculated, any of those physical properties, can be determined computationally, in principle. The methods that obtain the total energy of the system, and then by applying the laws of the quantum mechanics, starting exclusively with the atomic information of the constituents of the system (in the case of solids, the number of positively charged nucleus and the number of electrons), are termed as ab-initio or first principles methods.

Among the variety of ab-initio methods proposed, the density functional theory (DFT) has demonstrated to be an extremely successful approach for the description of the ground state properties of solids. The main idea behind the DFT is the possibility to describe the system by its electronic charge density, instead of using its complete many-body wave function [36]. The Kohn-Sham (KS) equations provide the way to convert the DFT a practical methodology [37]. The approximation within the DFT most used often is the local-density approximation (LDA), which locally substitutes the exchange-correlation energy on an inhomogeneous system by that of the homogeneous electron gas

2.2.1. Hohenberg-Kohn theorem

According to Hohenberg-Kohn theorem [37], the total energy functional can be written as follows

$$E[n] = F[n] + \int V_{ext}(r)n(r)d^3r, \quad (2.3)$$

where $V_{ext}(r)$ is external potential, the wave function is denoted by ψ, and the corresponding density is *n(r)*. Unfortunately, the Hohenberg-Kohn theorems do not provide the exact functional *F[n]*, and the problem of determining the ground state energy and density is subordinate to the discovery of sufficiently accurate estimations of such functional.

2.2.2. Kohn-Sham equations

Kohn-Sham equations establish the methodology for the practical use of the Hohenberg-Kohn theorems [37]. In these equations, the interacting electron system under the influence of the external potential is represented by a system of non-interacting electrons under the influence of a mean-field potential. This potential, called as KS potential $V_{KS}(r)$, is chosen in such a way that its ground state density is the same as for the interacting electron system. The one electron KS wave functions are then the solutions of the single-particle Schrodinger equation

$$\left\{-\frac{1}{2}\nabla^2 + V_{KS}(r)\right\}\psi_i(r) = \varepsilon_i\psi_i(r) \quad , \quad (2.4)$$

where ε_i are the energy eigen values. The potential $V_{KS}(r)$ includes the external potential and the electron-electron interaction. The density *n(r)* is written as

$$n(r) = \sum_{i=1}^{N}|\psi_i(r)|^2 \quad , \quad (2.5)$$

where only the N occupied (lowest energy) states participate in the construction of n(r). The exchange energy is due to the anti-symmetry of the many-electron wave function

that produces a spatial separation between electrons with the same spin, thus reducing the Coulomb energy of the system [38]. On the other side, the correlation energy comes from the difference between the many-body energy of an electronic system and the energy of the system calculated in the Hartree-Fock approximation [133]. Therefore, the potential $V_{KS}(r)$ is given by

$$V_{KS}(r) = V_{ext}(r) + \int \frac{n(r)}{|r-r'|} d^3r' + V_{XC} \quad . \tag{2.6}$$

The system of equations (2.4), (2.5) and (2.6) are known as Kohn-Sham equations.

By solving them self-consistently, the ground state density and the total energy of the system can be subsequently found [16]. In the following, the interaction of the electrons with the nuclei is introduced by means of the external potential. The Kohn-Sham equations are exact, and provide the exact ground state density. Moreover, the KS equations provide reliable solutions in reasonable computational times. However, all the benefits promised by this theoretical framework depend on the ability to deal with the exchange-correlation functional, in an exact rigorous manner or by means of finding accurate approximations.

2.2.3. Local-density approximation and the band gap problem

The simplest approximation, and also the most widely used to the exchange-correlation energy E_{XC}, is the local density approximation (LDA). LDA assumes that the exchange-correlation energy of a non-uniform system can be obtained by using the information obtained from the uniform electron gas. Therefore, effects of the inhomogeneity in the density on E_{XC} are ignored. Despite this gross oversimplification, it is remarkable the good results that the LDA has provided over the years [39]. This is so

to such an extent that DFT-LDA can be considered the cornerstone of most of the electronic structure calculations.

However, one of the major problems of LDA is that it systematically underestimates the band gap of semiconductors and insulators with respect to the experimental value. The band gap of a semiconductor is the difference between the ionization potential and electron affinity. For the correction of this underestimation of the band gap, a wealth of alternative approaches to LDA has been proposed [13]. Other approaches beyond DFT that are based in many-body perturbation theory and in the Green-function formalism, e. g., the GW approximation have demonstrated the capability to improve the LDA results [40]. However, these methods are much difficult of implementing and add a substantial increment in the computational time.

2.3. Plane wave pseudo potential method

In solid state physics, due to the periodicity of crystals, the Bloch's theorem establishes that the wave function of an electron with wave vector *k* in band *j*, $\psi_{j,k}(r)$, can be written as the product of a plane wave and a periodic function$u_{j,k}(r)$,

$$\psi_{j,k}(r) = e^{ik.r} u_{j,k}(r), \tag{2.7}$$

where *k* can be restricted without loss of generality to the first Brillouin zone (BZ) [144]. Since $u_{j,k}(r)$, has the periodicity of the crystal lattice, it can be expanded in a Fourier series of plane waves with wave vectors G belonging to the reciprocal lattice

$$u_{j,k}(r) = \sum_G A_{j,k}(G)\, e^{iG.r} \quad , \tag{2.8}$$

and the Bloch wave function of the electron can be expressed as follows

$$u_{j,k}(r) = \sum_G A_{j,k}(G)\, e^{i(k+G).r} = \sum_G A_{j,k}(G)\, \langle r|k+G\rangle \, , \tag{2.9}$$

where the plane waves $\langle r|k+G\rangle = \frac{1}{\sqrt{V}} e^{i(k+G).r}$ form an orthogonal basis

$$\langle G|G'\rangle = \delta_{G.G'}, \tag{2.10}$$

Therefore, the plane wave basis is specially suited for such periodic systems. Plane wave representation can be applied to the KS equations. But the important disadvantage of the plane wave basis is that they are non-localized functions, and it is required to use large basis sizes to deal with strongly oscillating functions (as the case of the atomic orbital) or very localized functions. This problem can be overcome by introducing the concept of pseudopotential [37]. In addition, the plane wave basis is in principle not suitable to deal with finite system. Therefore, in these cases, the use of a plane wave basis cannot take advantage of the interface to vacuum to reduce the basis size. In those cases, a large super cell is defined to enforce the periodicity of the system, but the super cell must be large enough to prevent coupling between different replicas of the system.

Before introducing the pseudopotentials, it is useful to split the electrons into core and valence electrons. This makes sense since most of the physical and chemical properties of crystals depend to a very good approximation only on the distribution of the valence electrons. Thus, the core electrons are strongly localized around the nucleus, interacting minimally with electrons from other atoms. It is therefore sensible to make the frozen core approximation that assumes the core electrons to be unperturbed by the environment. The contributions of the core electrons and nuclei are therefore combined into a single ionic pseudopotential. In this way, a great simplification is introduced into the KS equation, and the number of eigen values to be calculated now is substantially reduced.

In summary, the pseudopotential formulation allows us to avoid the use of the true atomic potential, and simplifies enormously the resolution of the KS equations. However, the best pseudopotential is a priori unknown, and the problem of determining such pseudopotential is not a trivial task. Since the works where the use of pseudopotentials was first proposed [36], the sophistication of the methodology to generate accurate and efficient pseudopotential has grown notably. Usually, the construction of pseudopotential starts from ab-initio calculations for an isolated atom. However, it is also desirable that pseudopotential is able to be used in other chemical environments, different from where it was generated. This property is the so-called transferability. The properties of softness and transferability are closely related to the cutoff radius r_c, and compete with each other. Thus, a low r_c gives pseudopotential very transferable, and on the other side, large r_c makes the pseudopotential softer. Therefore, one must find a compromise between the two requirements. The main types of pseudopotentials, among others, are Norm conservation pseudo potentials and Ultra-soft pseudopotentials

2.3.1. Norm conservation pseudo potentials

First, the pseudo wave function outside r_c must mimic the all electron wave function. Moreover, inside the sphere defined by the cutoff radius the pseudo wave function and the all electron wave function must have the same norm, in order to guarantee that both wave functions generate identical electron densities in the external region.

2.3.2. Ultra-soft pseudopotentials

Here the pseudo wave functions are required to be equal to the all electron wave functions for $r > r_c$ but the norm-conserving requirement is relaxed, and the pseudopotential for $r < r_c$ is allowed to be as soft as possible [41]

2.4. Band corrected pseudo potential scheme

As discussed in previous sections, plane wave pseudopotential LDA calculations give incorrect band gap. Therefore, to correct the pseudopotential, the nonlocal potentials of atoms are changed [13]. An extra $\beta \frac{sin\left(\frac{r\pi}{r_c}\right)}{r}$ potentials are added to the s, p, and d nonlocal potentials, with r_c fixed at 0.8–1.1 Å and β as the fitting parameters. We adopt a systematic approach to correct the critical point energies of the conduction bands at Γ, L and X points, the separation of the p and d orbital derived valence bands, and the position of VBM, using the six adjustable parameters for a binary compound. Furthermore, the corrections for cation In are common for all the In-V binaries. [Y. Zhang, unpublished]. The deformation potentials of the modified pseudopotentials, although not fitted, will follow closely the original LDA results. It is also reported in [13] that the charge transfer (self-consistency) from the cation to anion has a big effect.

In this correction scheme, after first obtaining the charge density and $V_{loc}(r)$ self-consistently, the modified nonlocal pseudopotential $\hat{V}'^{atom}_{nonloc}$ is used in the place of the original nonlocal pseudopotential. The single particle Schrodinger equation is then

$$\left[-\frac{1}{2}\nabla^2 + V_{loc}(r) + \sum_{atom,R} \hat{V}'^{atom}_{nonloc}(r-R)\right]\psi_i = E_i\psi_i \ , \qquad (2.11)$$

where R is the positions of the atoms.

Also energy of the valence band maximum (VBM) has to be fitted to its original LDA result to avoid altering the valence band alignment. This “band-corrected pseudopotential” approach has been used previously for the treatment of nanocrystals and isovalent impurities with great sucess [13] [17] [42] [43] .

CHAPTER 3: NUMERICAL SIMULATION

In this chapter we give details about the input parameters used for pseudopotential simulations. We begin with a summary of the plane wave pseudopotential code PEtot used. We also then discuss in more detail about the various terminologies related to the PEtot code.

3.1. PEtot

PEtot stands for Parallel Total Energy (Etot), is a parallel plane wave pseudopotential program for atomistic total energy calculation based on density functional theory. It simulates large systems on large parallel computers like IBM SP machines at NERSC, and linux cluster machines, under U.S. Department of Energy funding and it is a freely distributed public source code [44].

PEtot was initially developed by Dr. Lin-Wang Wang. Later parallelized by Lin-Wang Wang and Andrew Canning in 1999 which includes Andrew Canning's Parallel Fast Fourier Transformation (FFT) code designed for electronic structure calculations. In 2004, version 2 of the code incorporating ultrasoft pseudopotentials was released. Also, it has a k-point parallelization on top of the G-space parallelization. Hence, it can also calculate isolated cluster systems and slab systems without the periodic image potentials. In 2010, version 3 with three levels of parallelizations (G-vector, band index, k-points) was released.

Some of the important features [44] of this code that makes it as an ideal one for this work are

- It is a planewave pseudopotential code which uses both the norm conservation pseudopotentials and ultrasoft pseudopotentials.
- It is good for large scale electronic structure calculations
- It can do calculations for: LDA, LSDA, GGA, although without spin-orbit coupling.

3.2. Description of PEtot inputs

PEtot_AllBand_BP3 (the main program), kpt_gen (the k-point generator), by James E. Bernard and Sverre Froyen; PSEUDO, the supporting pseudopotential generating package from J.L. Martin with modifications; ULTRASOFT, the ultrasoft pseudopotential package from D. Vanderbilt without any modifications; VWR_ALL_ATOM (the norm conserving pseudopotential library, generated from PSEUDO); USSP_TXT_ALL (the ultrasoft pseudopotential library, generated from ULTRASOFT)

The unit cell considered consists of two atoms of group V (P, As, Sb) at [0,0,0], and an atom of In at $\left[\frac{a}{4},\frac{a}{4},\frac{a}{4}\right]$, where a is the lattice constant. Norm conserving pseudopotentials from VWR_ALL_ATOM, the norm conserving pseudopotential library are used. To study the InV (V=P, As, Sb) compounds, s, p and d states were considered as valence states. The semicore d-electrons of these compounds have been included into the core, because the energy level of the d-electrons are relatively close to the outermost sp-levels [45] and the electrons are expected to affect significantly on the band structures of the compounds.

We have used 4.7 as r_{cut} which is a safe number. As per [44], since, a larger r_{cut} will give more accurate of the KBS real space implementation, but computation is more costly. The Ecut is usually determined by the pseudopotentials. The vwr.atom file of norm conserving pseudopotential library has the converged Ecut for each atom. An Ecut of 60 Ryd is used for all the simulations.

The Pulay Kerker scheme has been used for self-consistent potential mixing. Also, g-space Kleinman Bylander non-local pseudopotential implementations have been used with maskr function scheme, without the need for preprocessing of the pseudopotentials. The LDA exchange-correlation contribution is accounted for by means of Perdew and Zunger's parametrization [46] of the calculations by Ceperley and Alder [47]. The self-consistent solution of the one-electron Kohn Sham equation has been performed by the planewave pseudopotential algorithm [39].

3.2.1. kpt_gen

Table 3.1 gives the input parameters used for kpt_input file. atom.config is the name of the atom.config file.

Table 3.1 Inputs of the kpt_input file

	InP	**InAs**	**InSb**
atom.config	xatom.InP	xatom.InAs	xatom.InSb
a_0	11.08466	11.4487	12.24391
V(1), V(2), V(3)	8	8	8
kshift(i)	1	1	1

a_0 is the cubic lattice constant of the crystal (in atomic unit Bohr). v(1), v(2), v(3) are the lattice vectors of AL(3,3) in atom.config. kshift(i) specifies whether you want a

half grid point shift in this ith-direction on the k-point grid. Sometime a shift can reduce the number of the reduced k-point in kpt.file. Sample kpt_input file can be seen in appendix A.

3.2.2. atom.config

Table 3.2 gives the input parameters used for atom.config file. natom is the number of atom in this system. AL (i) the ith edge vector of the supercell (in atomic unit Bohr). iatom is the atomic number from the periodic table, assigned to each atom pseudopotential file vwr.atom in the norm conserving pseudopotential library.

Table 3.2 Inputs of the atom.config file

	InP	**InAs**	**InSb**
Natom	2	2	2
AL(i)	5.54233	5.72435	6.121955
	For V (P As, Sb) atom		
Iatom	15	33	51
x1,x2,x3	0.0,0.0,0.0	0.0,0.0,0.0	0.0,0.0,0.0
im1,im2,im3	0,0,0	0,0,0	0,0,0
	For In atom		
Iatom	49	49	49
x1,x2,x3	0.25,0.25,0.25	0.25,0.25,0.25	0.25,0.25,0.25
im1,im2,im3	0,0,0	0,0,0	0,0,0

x1,x2,x3 is the atomic position in the unit of edge vector AL(1),AL(2),AL(3). im1, im2, im3 tells whether to move the atom in x, y, z direction. 0 will not move and 1 will move in that direction. Sample kpt_input file can be seen in appendix B.

3.3. Input parameters

The lattice constants have been reported as 5.86575 Å (10 K), 6.0584 Å (10 K), and 6.4792Å (10 K) at lowest available temperature for InP [48], InAs [49] and InSb [50]

respectively. For fitting the pseudopotentials, energies at (critical points) *Γ, X, and L* in the Brillouin zone are required. These values can be found in table 3.3.

Table 3.3 Energies at critical points in Brillouin zone. Theoretical energies are quasiparticle energies [51]. Energies are in eV

	InP		**InAs**		**InSb**	
	Expt	Theory	Expt	Theory	Expt	Theory
$\mathbf{\Gamma_{1C}}$	1.4236 [48]	1.44	0.418 [49]	0.31	0.2352 [50]	0.08
$\mathbf{X_{1C}}$	2.38	2.58		2.01	1.79	1.50
$\mathbf{X_{3C}}$		3.08		2.50		1.57
$\mathbf{L_{1C}}$	2.03	2.28	1.55	1.43		0.76
$\mathbf{E_{p\text{-}d}}$	16.80 [45]		17.09 [45]		17.29 [45]	

Valence Band Maximum (*VBM)* is zero, as the energy reference, in all the cases. *1C* is the first conduction band and the *3C* is the second conduction band. $E_{p\text{-}d}$ is the energy difference between the *VBM* and d orbital derived valence band and the experimental values are found using XPS spectroscopy [51]. For any experimentally unavailable values, quasiparticle energies have been used [51]. As said in the earlier chapter, quasiparticle band structure is much more accurate but the method cannot be used for larger systems. Eigen energies generated using non-self-consistent calculations will be fit by adding extra potentials to the nonlocal part of the atomic pseudopotentials.

3.4. Procedure

The steps followed to systematically correct the bandgap errors in density-functional-theory band structure calculations for InV (V = P, As, Sb) are

1) Self-consistent calculation:

Energy cut, *Ecut* of 60 Ry and k space grid of 8x8x8 is used. The kpt_gen code generates 60 k points and 24 symmetry operations. At the end of self-consistent calculation, the charge density and potential files are generated.

2) Band structure calculation:

Using the generated potential and charge density, eigen energies at the special k points (Γ, X, and L points) were found by non-self-consistent calculations. Because spin-orbital coupling Δ_{SO} is not taken into account by PEtot code, in our fitting *VBM* and $E_{p\text{-}d}$ are adjusted by subtracting $\frac{\Delta_{SO}}{3}$, 0.036 eV, 0.13 eV, and 0.27 eV for InP, InAs, and InSb [52], respectively.

The process of modifying the nonlocal part of the atomic pseudopotential is developed by Dr. Lin-Wang Wang. A Fortran code, "chvwratom.f is used to add the extra $\beta \frac{sin\left(\frac{r\pi}{r_c}\right)}{r}$ potentials to the s, p, and d nonlocal potentials. A procedure to correct simultaneously all the binaries such as In-V (V = P, As, Sb) has been developed by Dr. Yong Zhang.

a. The p-d separation $E_{p\text{-}d}$ are fitted to experimental value by changing d component of the cation (In) pseudopotential. An average of the In-d orbital corrections for different binaries, which are relatively close to each other, is used for the next step.
b. The calculated energy at X_{1C} and X_{3C} can be fitted to experimental value by changing the p orbital of the cation (In) and the d orbital of the anion V (V=P, As, Sb).

c. The valence band maximum (VBM) of InV (V=P, As, Sb) are fitted by adjusting the p orbital of the anion V.

d. Adjusting the s orbital of the cation (In) and anion V (V=P, As, Sb), the Γ_{1C} (CBM) and X_{1C}, X_{3C} and L_{1C} are fitted to experimental values.

For a value of In-s orbital correction, V-s orbital correction values are adjusted to fit Γ_{1C} (CBM) to the experimental value. Then In-s orbital correction is changed and V-s orbital correction values are adjusted to fit Γ_{1C} (CBM) to the experimental value. So we have a set of In-s orbital correction and their corresponding adjusted V-s orbital correction values. Then a final value of In-s and V-s is obtained using the following equation.

Γ_{1C} (In-s) + Γ_{1C} (P-s) = Experimental Γ_{1C} (CBM), (3.1)

Similarly for InAs and InSb, we have

Γ_{1C} (In-s) + Γ_{1C} (As-s) = Experimental Γ_{1C} (CBM), (3.2)

Γ_{1C} (In-s) + Γ_{1C} (Sb-s) = Experimental Γ_{1C} (CBM), (3.3)

So, simultaneously for all the binaries, the above equation is solved to find a good fitting of In-s orbital correction. Similar equations can be used fitting energies at X and L level to their corresponding experimental values.

The energies at the critical points are fitted to the experimental value by modifying the nonlocal part of the atomic pseudopotential. The modified pseudopotential can be used for larger systems to elucidate its electronic band structure and other properties.

CHAPTER 4: RESULTS AND DISCUSSION

In this chapter, we discuss the results of band corrected pseudopotential scheme to correct the band gap of InV (V=P, As, Sb) semiconductors. We begin with the self-consistent calculation of complete InV (V=P, As, Sb) semiconductors. We then calculate the DFT-LDA band structure at the main symmetry points of InV (V=P, As, Sb) and compare it to experimental values. Finally we conclude with a discussion of the comparison of electronic band structure before and after correcting the band gap errors.

4.1. Self-consistent calculation

The lattice constants 5.86575 Å (10 K), 6.0584 Å (10 K), and 6.4792Å (10 K) at lowest available temperature for InP [6], InAs [7] and InSb [8] respectively are used for the self-consistent calculation. Energy cutoff, *Ecut* of 60 Ry and k space grid of 8x8x8 is used. The kpt_gen code generates 60 k points and 24 symmetry operations. At the end of self-consistent calculation, the charge density and local potential files are generated.

As discussed in the previous chapter, using the generated local potential and charge density, eigen energies at the special k points (Γ, X, and L points) were found by non-self-consistent calculations. Because spin-orbital coupling Δ_{SO} is not taken into account by PEtot code, in our fitting *CBM* (Γ_{1C}), X_{1C}, X_{3C} and L_{1C} are adjusted by subtracting $\frac{\Delta_{SO}}{3}$, 0.036 eV, 0.13 eV, and 0.27 eV for InP, InAs, and InSb [10], respectively. The energies at the critical points are tabulated in table 4.1. The target

values are from table 3.3 (Chapter 3) after adding Δ_{SO} correction to the band gaps. As discussed in previous chapter, for any experimentally unavailable values, quasiparticle energies [9] have been used as the target values.

Table 4.1 Energies at critical points in Brillouin zone. Theoretical energies are from DFT-LDA calculations before pseudopotential fitting. Energies are in eV

	InP		**InAs**		**InSb**	
	Target	Theory	Target	Theory	Target	Theory
$\mathbf{\Gamma_{1C}}$	1.4596	0.3902	0.548	-0.4293	0.5052	-0.4711
$\mathbf{X_{1C}}$	2.416	1.6068	2.14	1.4387	2.06	1.2535
$\mathbf{X_{3C}}$	3.116	2.1000	2.63	1.9144	2.13	1.2606
$\mathbf{L_{1C}}$	2.066	1.2392	1.68	0.7614	1.03	0.3645
$\mathbf{E_{p\text{-}d}}$	16.80	14.331	17.09	14.4943	17.29	14.6474

The current plane wave pseudopotential LDA calculations give band gaps of 0.3902 eV, -0.4293 eV and -0.4711 eV for bulk InP, InAs and InSb, respectively, while the experimental band gaps are 1.4326 eV, 0.418 eV and 0.2352 eV. The negative value of InAs and InSb band gap shows that CBM is below than VBM, which is not correct as a result of LDA. Similarly, calculated energies at X and L points are also different from the target values.

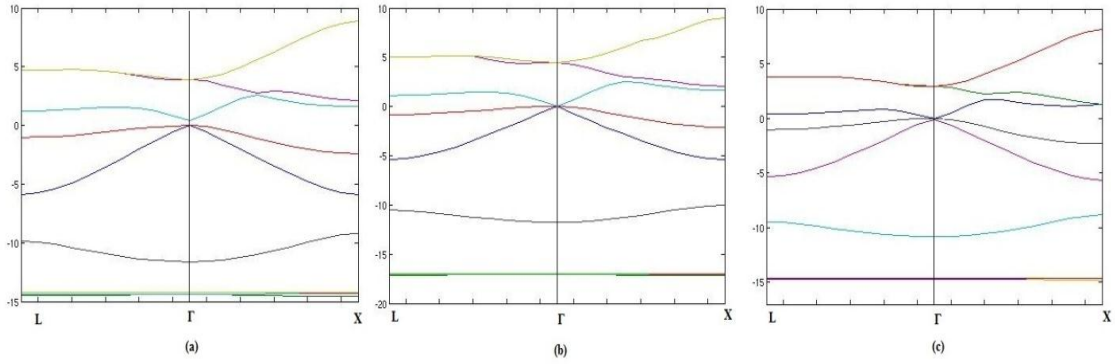

Figure 4.1 Band structure of a) InP b) InAs and c) InSb from DFT-LDA calculation

Therefore, to correct these band gap errors, nonlocal part of the atomic pseudopotentials are modified. The full band structure of InP, InAs & InSb from DFT-LDA calculations before correcting the atomic pseudopotential is shown in figure 4.1. Hence, the band gap errors of DFT-LDA calculations have to be corrected systematically, by changing the non-local part of the atomic pseudopotentials.

4.2. In – d Fitting

A Fortran code "chvwratom.f", is used to add the extra $\beta \frac{sin\left(\frac{r\pi}{r_c}\right)}{r}$ potentials to the s, p, and d nonlocal potentials. First, d orbital of cation (In) pseudopotential is adjusted to fit the p-d separation $E_{p\text{-}d}$. Using the Fortran code "chvwratom.f" , corrections to d orbital of cation (In) are added and the energy at the critical points are generated. In-d orbital correction value is changed and the corresponding energies at the critical points are generated for InV(V= P, As, Sb). Figure 4.2 is a plot between calculated $E_{p\text{-}d}$ vs. In-d orbital correction of InP.

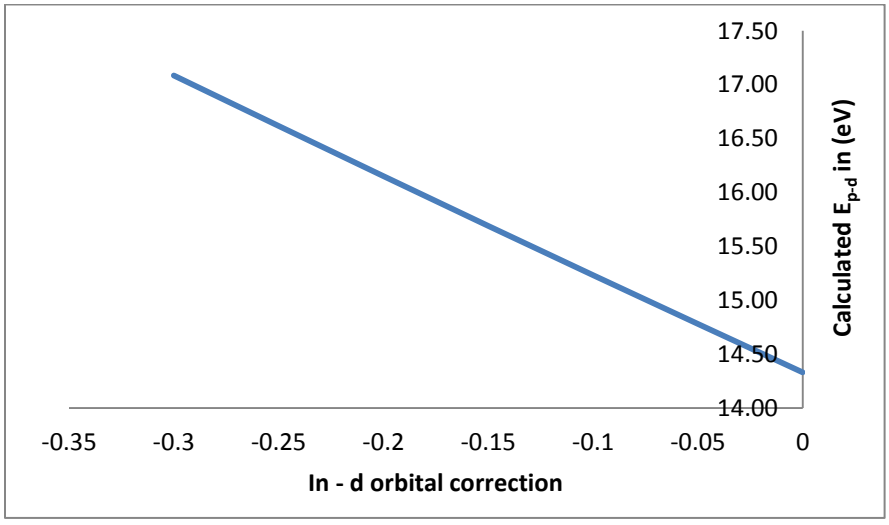

Figure 4.2 Plot between calculated $E_{p\text{-}d}$ vs. In-d orbital correction of InP

From the figure 4.2, it is clear that on changing the In-d orbital correction, $E_{p\text{-}d}$ changes linearly. Similarly, for InAs and InSb the plot between calculated $E_{p\text{-}d}$ vs. In-d orbital correction varies linearly (Figure 4.3 & Figure 4.4).

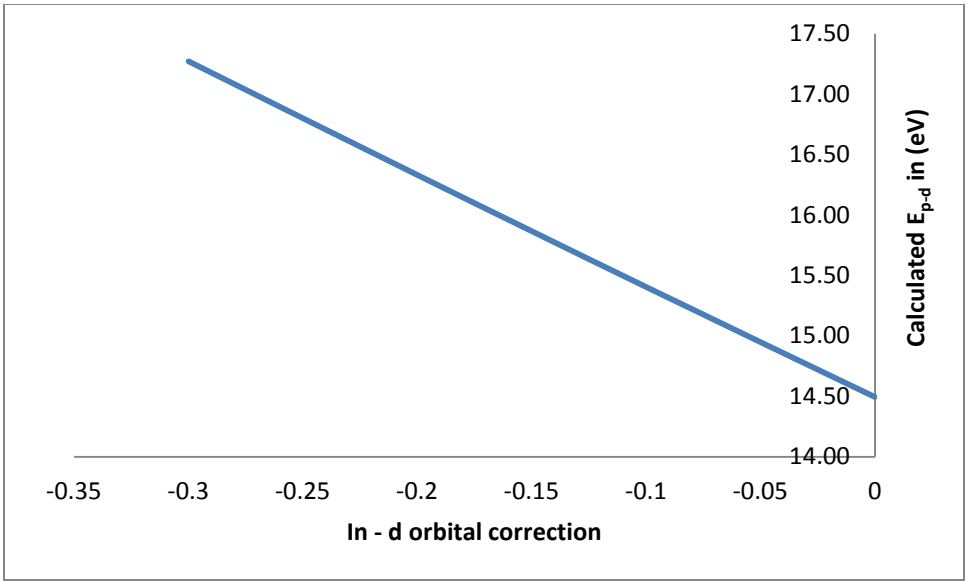

Figure 4.3 Plot between calculated $E_{p\text{-}d}$ vs. In-d orbital correction of InAs

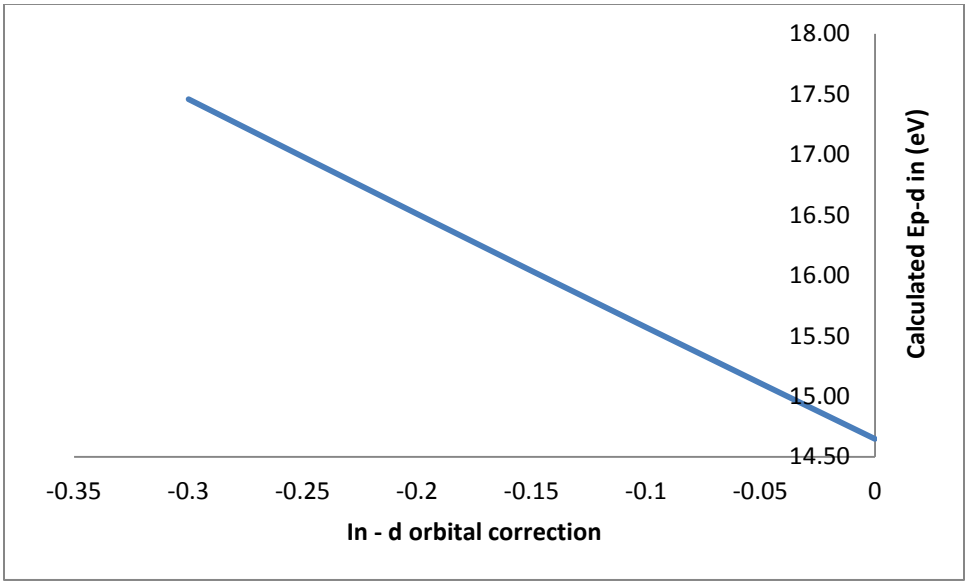

Figure 4.4 Plot between calculated $E_{p\text{-}d}$ vs. In-d orbital correction of InSb

Now, the value of In-d orbital correction at which the calculated $E_{p\text{-}d}$ is same as the experimental $E_{p\text{-}d.}$ is needed. A linear curve fitting of the In-d orbital correction vs. the difference between calculated $E_{p\text{-}d}$ and target $E_{p\text{-}d}$ is plotted for InP (Figure 4.5), InAs (Figure 4.6) and InSb (Figure 4.7).

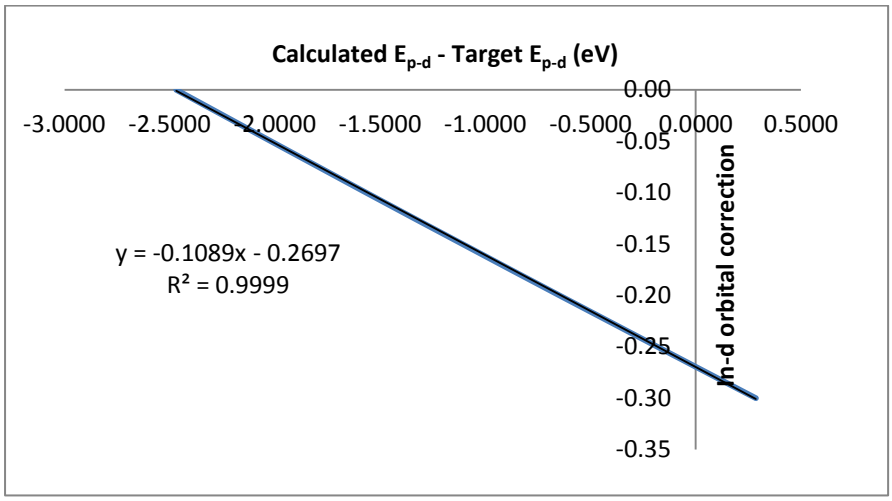

Figure 4.5 Plot between In-d orbital correction vs. the difference between calculated $E_{p\text{-}d}$ and target $E_{p\text{-}d}$ of InP

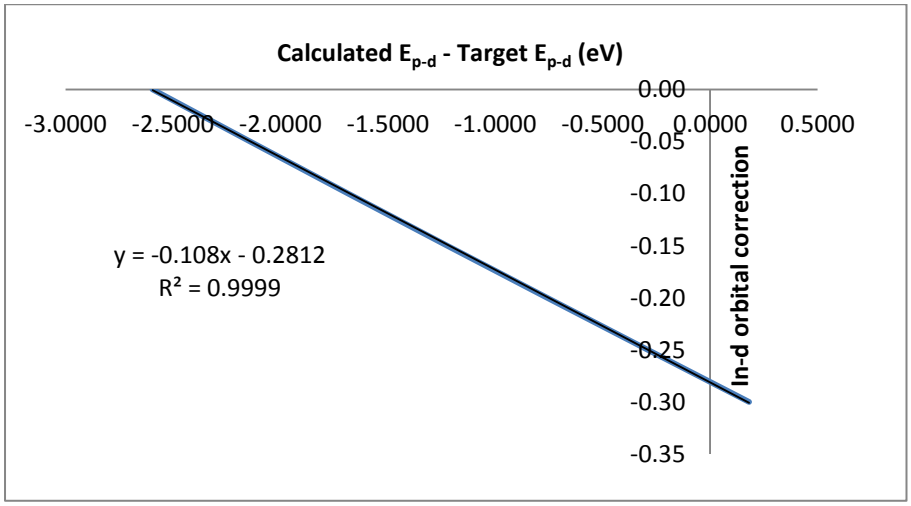

Figure 4.6 Plot between In-d orbital correction vs. the difference between calculated $E_{p\text{-}d}$ and target $E_{p\text{-}d}$ of InAs

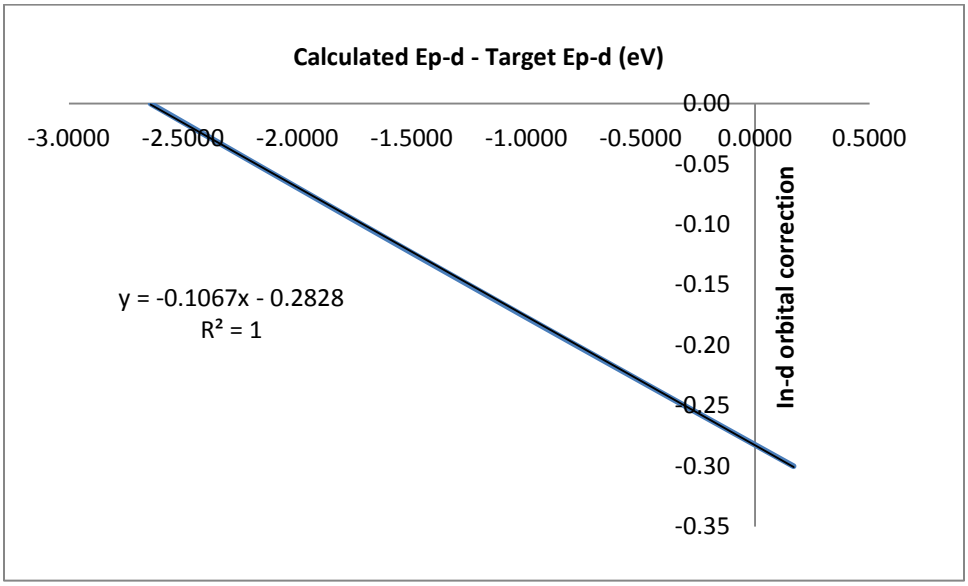

Figure 4.7 Plot between In-d orbital correction vs. the difference between calculated $E_{p\text{-}d}$ and target $E_{p\text{-}d}$ of InSb

We know that the linear equation is,

$$y = mx + c \quad , \quad (4.1)$$

and constant c is the value of y when x is zero.

Using this property of linear equation, we can find the value of In-d correction at which difference between calculated $E_{p\text{-}d}$ and target $E_{p\text{-}d}$ is zero, which is nothing but the In-d correction value when the calculated $E_{p\text{-}d}$ is same as the target $E_{p\text{-}d}$. In summary, In-d orbital corrected value is -0.2697 for InP, -0.2812 for InAs and -0.2828 for InSb. An average of these three values -0.2779 is the In-d orbital corrected value will be used for further calculations.

4.3. In – p Fitting

Next, p orbital of cation (In) pseudopotential is adjusted to fit the energy at X_{1C} and X_{3C}. Using the Fortran code “chvwratom.f” , corrections to p orbital of cation (In),

are added and the In-d orbital correction as -0.2779 from the previous step is used. Energies at the critical points are generated. Similar to the previous step, In-p orbital correction value is changed and the corresponding energies at the critical points are generated for InV(V= P, As, Sb). Figure 4.8 is a plot between calculated X_{1C} and X_{3C} vs. In-p orbital correction of InP.

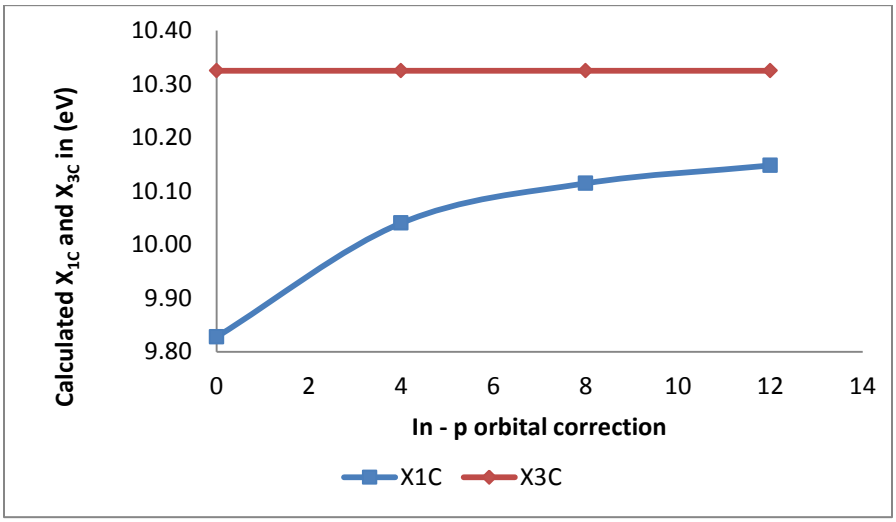

Figure 4.8 Plot between calculated X_{1C} and X_{3C} vs. In-p orbital correction of InP

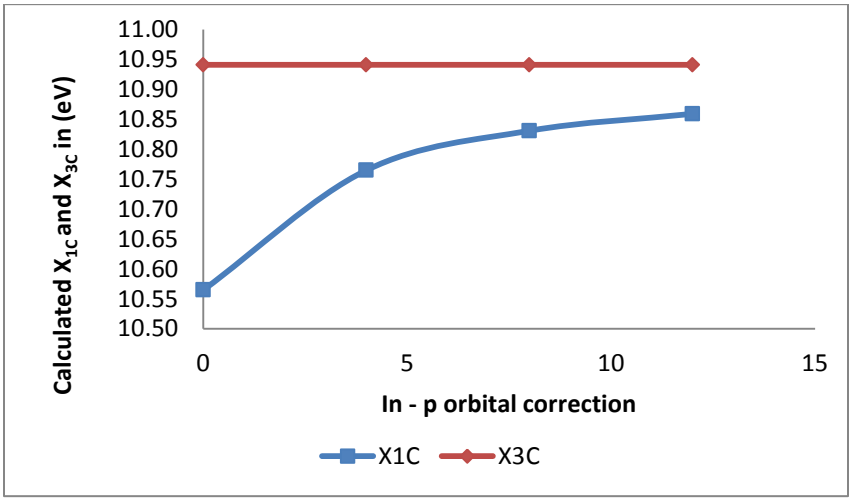

Figure 4.9 Plot between calculated X_{1C} and X_{3C} vs. In-p orbital correction of InAs

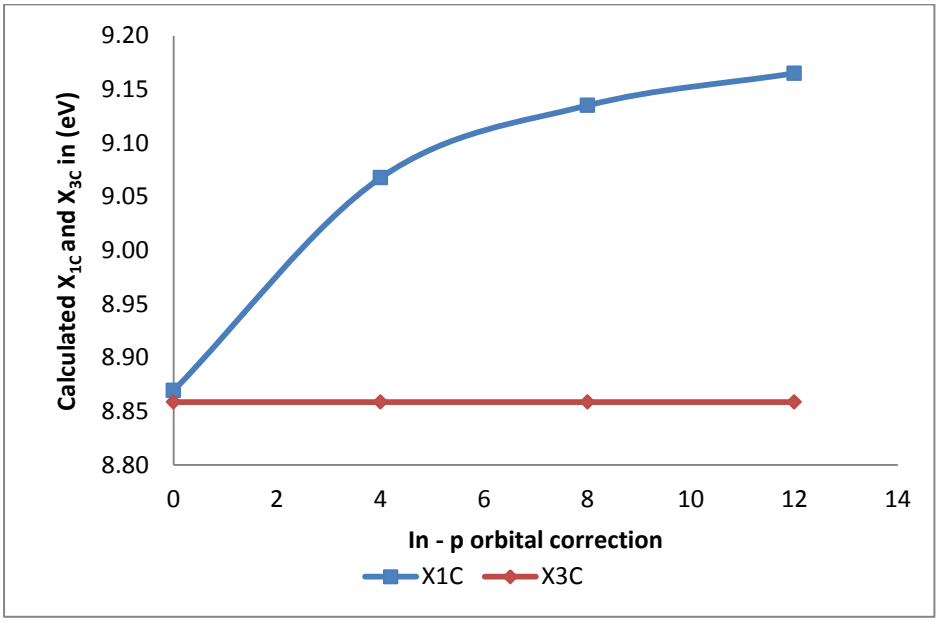

Figure 4.10 Plot between calculated X_{1C} and X_{3C} vs. In-p orbital correction of InSb

From the figure 4.8, 4.9 and 4.10, it can be observed that for InP, InAs, and InSb X_{1C} varies exponentially and X_{3C} remains constant.

To avoid altering the valence band alignment, all the energies are referred to their corresponding LDA results VBM value after fitting d orbital of cation (In).

Table 4.2 Energies at critical points in Brillouin zone after fitting d orbital of cation (In) Energies are in eV

	InP		**InAs**		**InSb**	
	Old Target	New Target	Old Target	New Target	Old Target	New Target
VBM	0.0	8.18798	0.0	8.88483	0.0	7.58184
Γ_{1C}	1.4596	9.64758	0.548	9.43283	0.5052	8.08704
X_{1C}	2.416	10.604	2.14	11.0248	2.06	9.64184
X_{3C}	3.116	11.304	2.63	11.5148	2.13	9.71184
L_{1C}	2.066	10.254	1.68	10.5648	1.03	8.61184
E_{p-d}	16.80	16.80	17.09	17.09	17.29	17.29

After fitting d orbital of In, LDA results VBM value 8.18798, 8.88483, and 7.5818 for InP, InAs and InSb respectively are added to target bandgaps and VBM. The new target values are tabulated in table 4.2. Now, the value of In-p orbital correction at which the calculated X_{1C} and X_{3C} is the same as the experimental X_{1C} and X_{3C} respectively, is needed. Since the relationship is exponential, we can use the value of In-p orbital correction at which the calculated X_{1C} and X_{3C} is closer to the target X_{1C} and X_{3C} respectively. From the figure 4.8, 4.9 and 4.10, In-p orbital corrected value is 8 for InP, 8 for InAs and 8 for InSb at which the calculated X_{1C} and X_{3C} is closer to the target X_{1C} and X_{3C} respectively. An average of these three values 8 is the In-p orbital corrected value will be used for further calculations.

4.4. V (V=P, As, Sb) – d Fitting

Next, d orbital of anion (V=P, As, Sb) pseudopotential is adjusted to fit the energy at X_{1C} and X_{3C}. Using the Fortran code "chvwratom.f", corrections to d orbital of anion (V=P, As, Sb), are added.

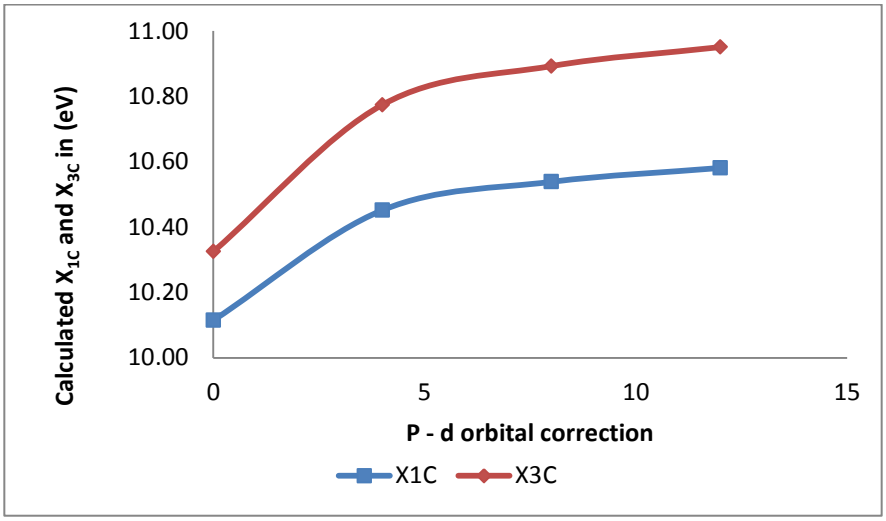

Figure 4.11 Plot between calculated X_{1C} and X_{3C} vs. P-d orbital correction of InP

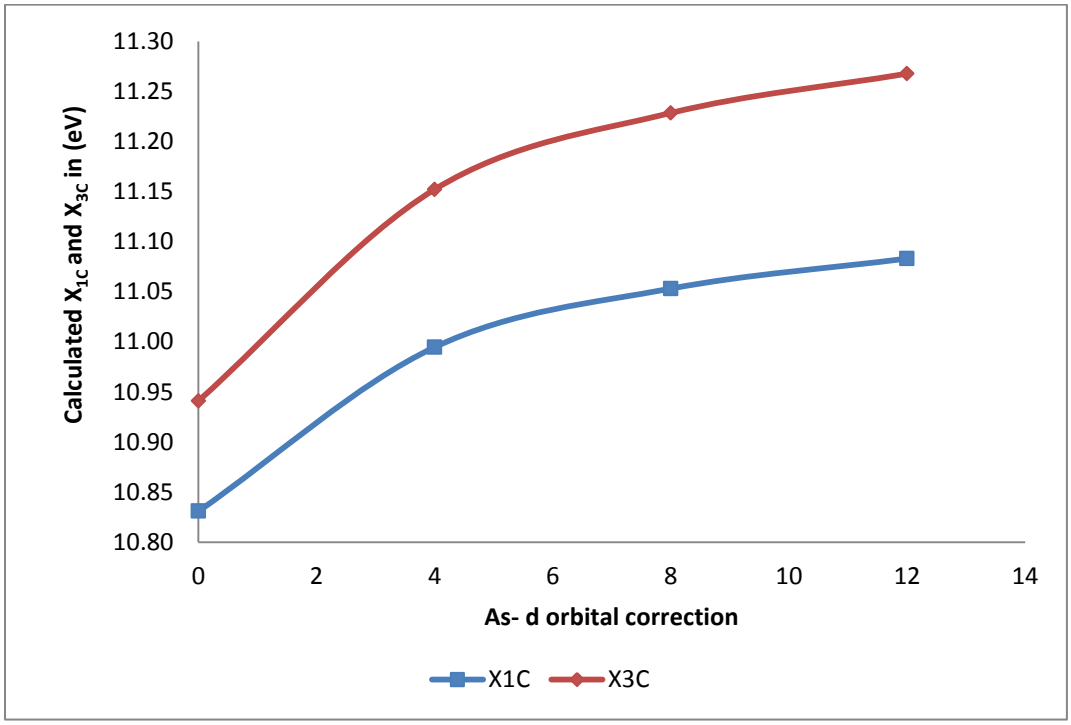

Figure 4.12 Plot between calculated X_{1C} and X_{3C} vs. As-d orbital correction of InAs

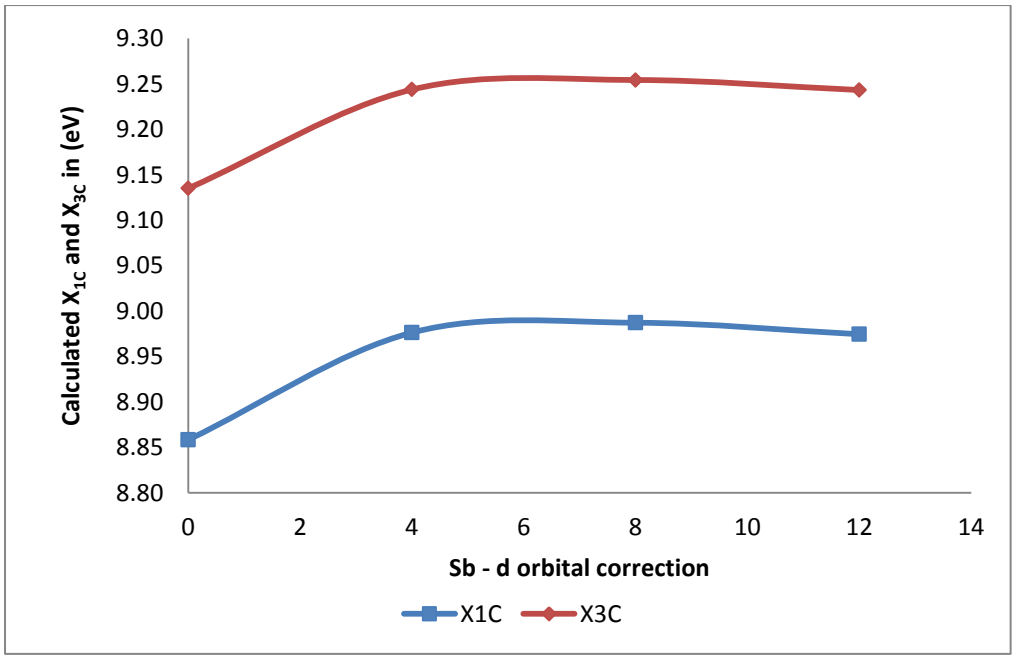

Figure 4.13 Plot between calculated X_{1C} and X_{3C} vs. Sb-d orbital correction of InSb

In-d orbital correction as -0.2779 and In-p orbital correction as 8 from the previous steps is used. Energies at the critical points are generated. Similar to the previous step, anion (V=P, As, Sb) orbital correction value is changed and the corresponding energies at the critical points are generated for InV (V= P, As, Sb). Figure 4.11 is a plot between calculated X_{1C} and X_{3C} vs. P-p orbital correction of InP.

From the figure 4.11, 4.12 and 4.13, it can be observed that for InP, InAs and InSb, X_{1C} and X_{3C} varies exponentially. Now, the value of anion-d orbital correction at which the calculated X_{1C} and X_{3C} is the same as the experimental X_{1C} and X_{3C} respectively, is needed. Since the relationship is exponential, we can use the value of In-p orbital correction at which the calculated X_{1C} and X_{3C} is closer to the target X_{1C} and X_{3C} respectively as in table 4.2. From the figure 4.11, 4.12 and 4.13, V(V=P, As, Sb)-p orbital corrected value is 8 for InP, 8 for InAs and 8 for InSb at which the calculated X_{1C} and X_{3C} is closer to the target X_{1C} and X_{3C} respectively. These values will be used for further calculations.

4.5. V(V=P, As, Sb) – p Fitting

Next p orbital of anion (V=P, As, Sb) pseudopotential is adjusted to fit the VBM. Using the Fortran code “chvwratom.f”, corrections to p orbital of anion (V=P, As, Sb) are added. In-d orbital correction as -0.2779, In-p orbital correction as 8, P-d orbital correction as 8, As-d orbital correction as 8 and Sb-d orbital correction as 8 from the previous steps is used. Energies at the critical points are generated. V (V=P, As, Sb)-p orbital correction value is changed and the corresponding energies at the critical points are generated for InV(V= P, As, Sb). Figure 4.14 is a plot between calculated *VBM* vs. P-p orbital correction of InP. From the figure 4.14, it is clear that on changing the P-p

orbital correction, *VBM* changes linearly. Similarly, for InAs and InSb the plot between calculated *VBM* vs. V (V=As, Sb)-p orbital correction varies linearly (Figure 4.15 & Figure 4.16).

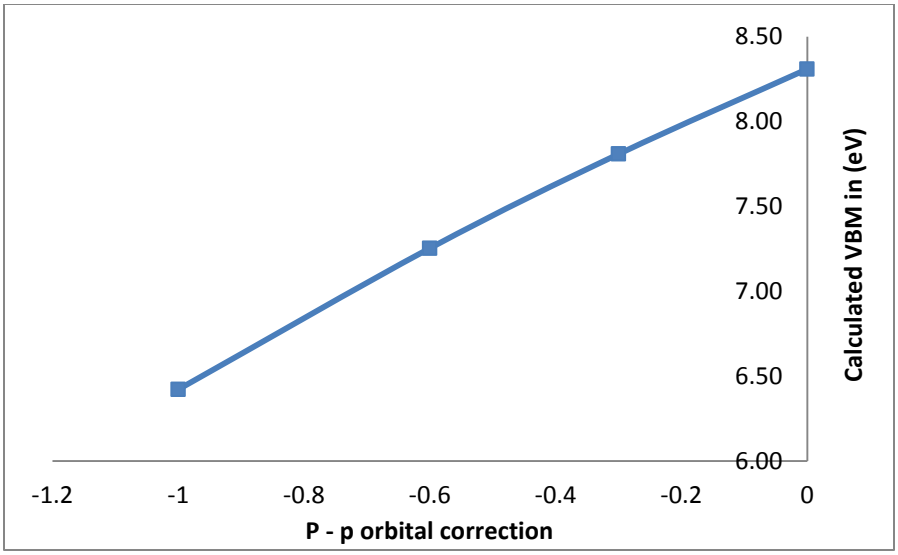

Figure 4.14 Plot between calculated *VBM* vs. P-p orbital correction of InP

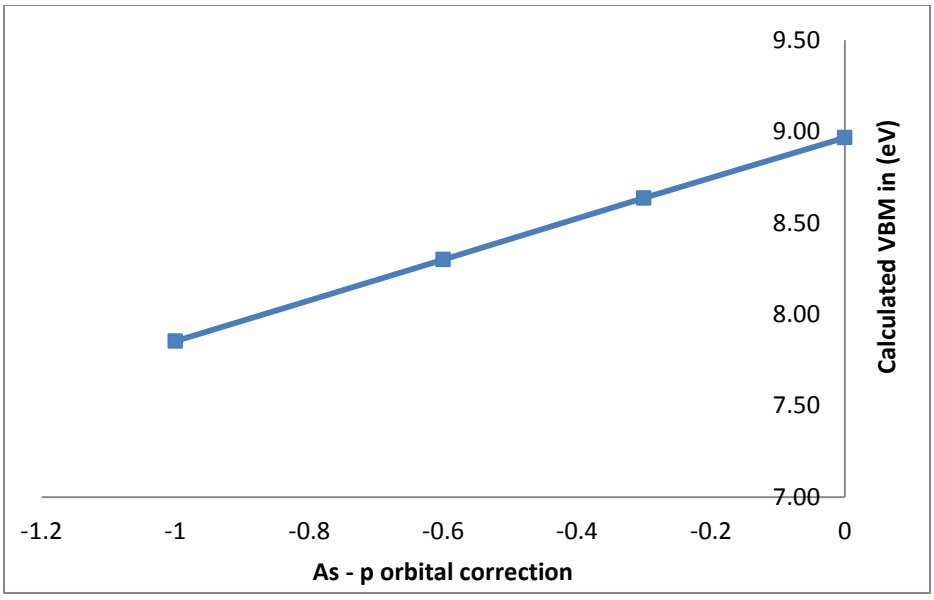

Figure 4.15 Plot between calculated *VBM* vs. As-p orbital correction of InAs

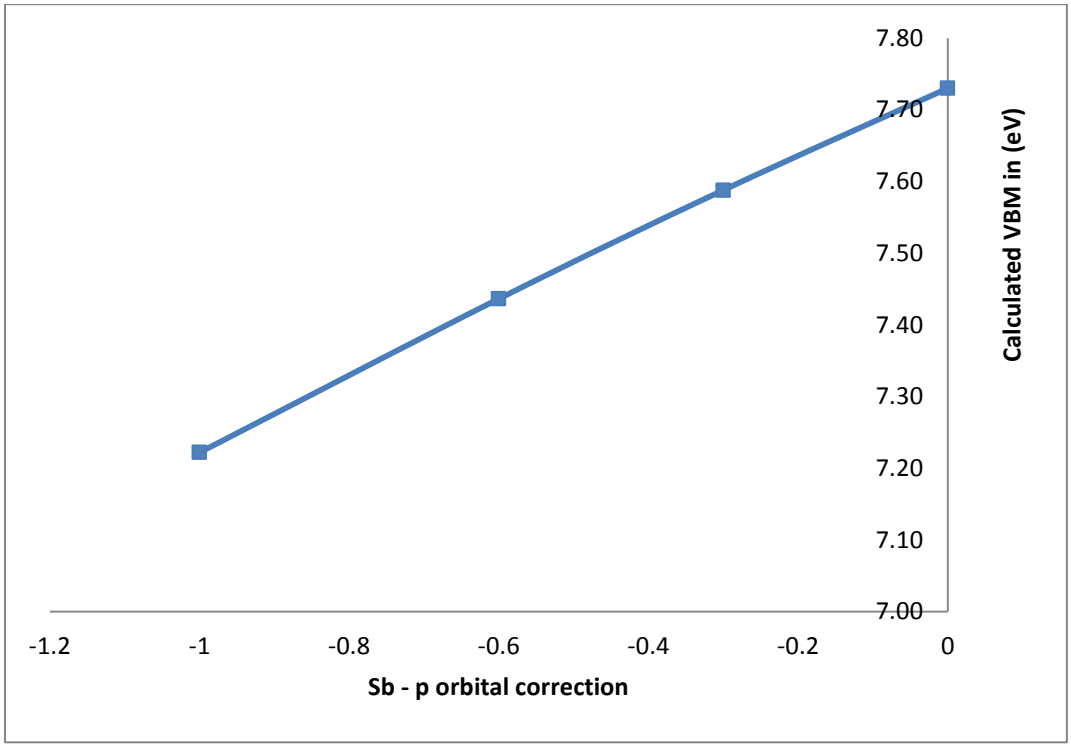

Figure 4.16 Plot between calculated *VBM* vs. Sb-p orbital correction of InSb

Now, the value of anion-p orbital correction at which the calculated *VBM* is same as the experimental *VBM*, as in table 4.2 is needed. As stated earlier in this chapter, since the relationship is linear, we can find the value of V (V=P, As, Sb)-p orbital correction at which difference between calculated *VBM* and target *VBM* is zero, which is nothing but the V (V=P, As, Sb)-p orbital correction value when the calculated *VBM* is same as the target *VBM*. In summary, V (V=P, As, Sb)-p orbital corrected value is -0.085 for InP, -0.0748 for InAs and -0.3029 for InSb. These values of V (V=P, As, Sb)-p orbital correction will be used for further calculations. A linear curve fitting of the V (V=P, As, Sb)-p orbital correction vs. the difference between calculated *VBM* and target *VBM* is plotted for InP (Figure 4.17), InAs (Figure 4.18) and InSb (Figure 4.19).

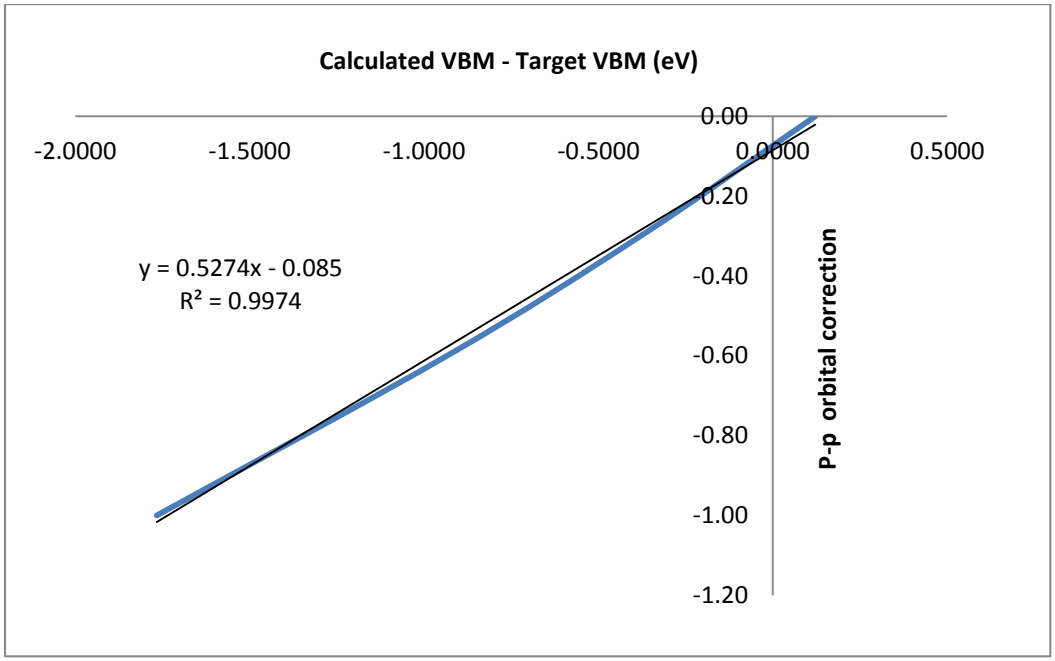

Figure 4.17 Plot between P-p orbital correction vs. the difference between calculated *VBM* and target *VBM* of InP

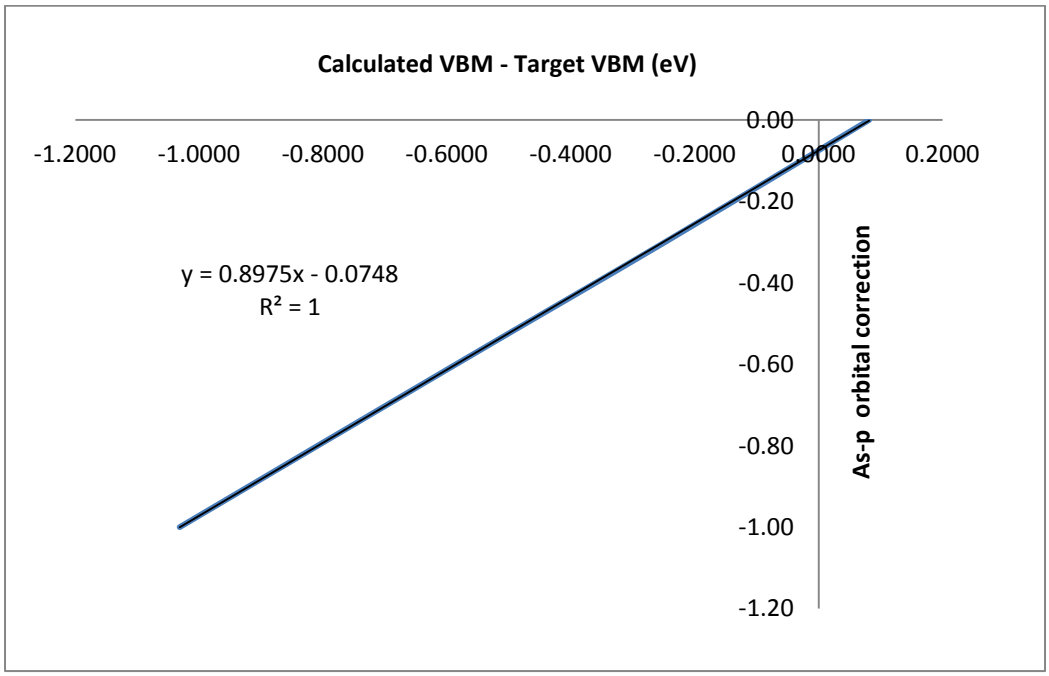

Figure 4.18 Plot between As-p orbital correction vs. the difference between calculated *VBM* and target *VBM* of InAs

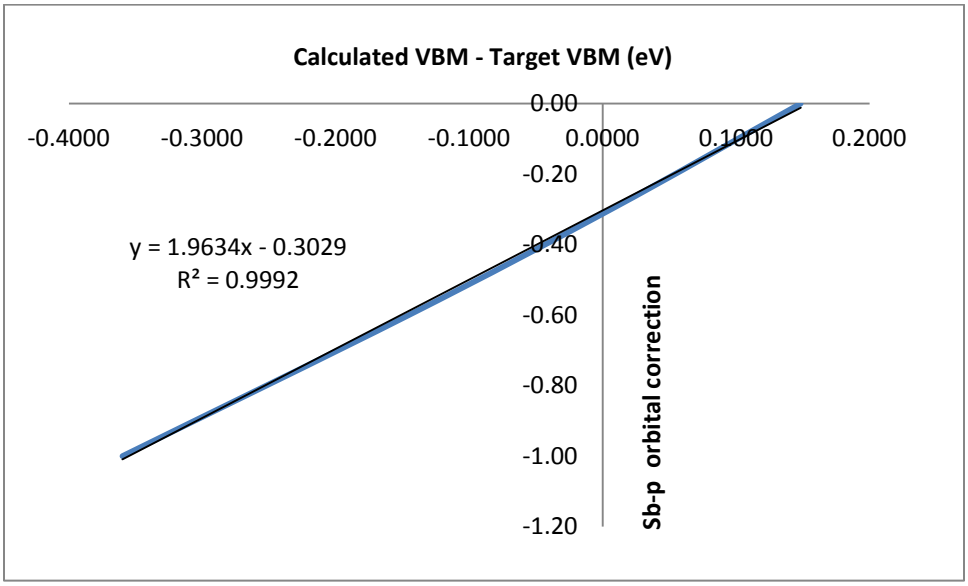

Figure 4.19 Plot between Sb-p orbital correction vs. the difference between calculated *VBM* and target *VBM* of InSb

4.6. In-s and V(V=P, As, Sb) – s Fitting

Next s orbital of cation (In) and anion (V=P, As, Sb) pseudopotential is adjusted to fit the Γ_{1C} (CBM), X_{1C}, X_{3C} and L_{1C}. Table 4.3 summarizes the corrections from the previous step used in this step.

Table 4.3 Summary of the anion and cation, p and d orbital correction from previous steps

	InP	**InAs**	**InSb**
In-d	-0.2779	-0.2779	-0.2779
In-p	8	8	8
V-d	8	8	8
V-p	-0.085	-0.0748	-0.3029

Using the Fortran code “chvwratom.f”, for a value of In-s orbital correction, V-s orbital correction values are added. Then In-s orbital correction is changed and V-s orbital

correction values are adjusted to fit Γ_{1C} (CBM) to the experimental value. So we have a set of In-s orbital correction and their corresponding adjusted V-s orbital correction values. Then by simultaneously solving the equations (3.1), (3.2) and (3.3), In-s orbital correction can be found. Energies at X and L level are also compared to their corresponding experimental values to get a good fit.

4.6.1. P-s Fitting

For a In-s orbital correction value, P-s orbital correction value is changed and the energies at critical points are generated. Figure 4.20 is a plot between calculated *CBM* vs. P-s orbital correction of InP with In-Vs as 0.0.

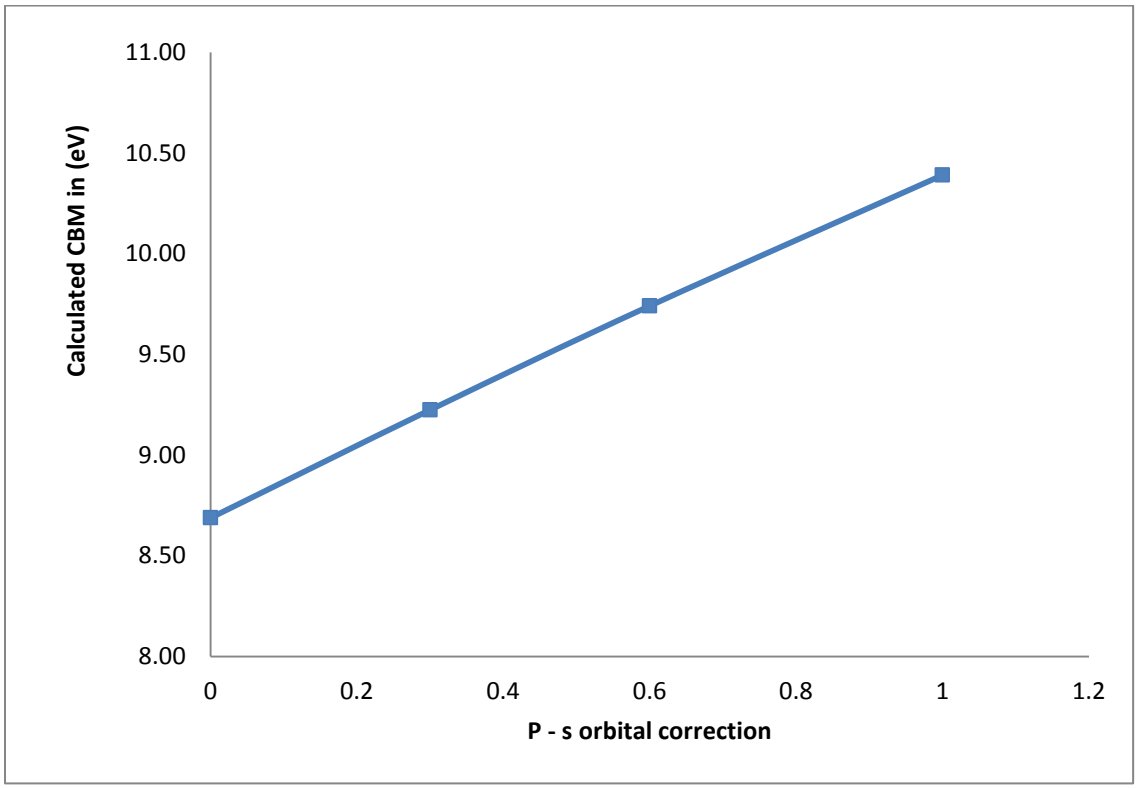

Figure 4.20 Plot between calculated *CBM* vs. P-p orbital correction of InP with In-s as 0.0

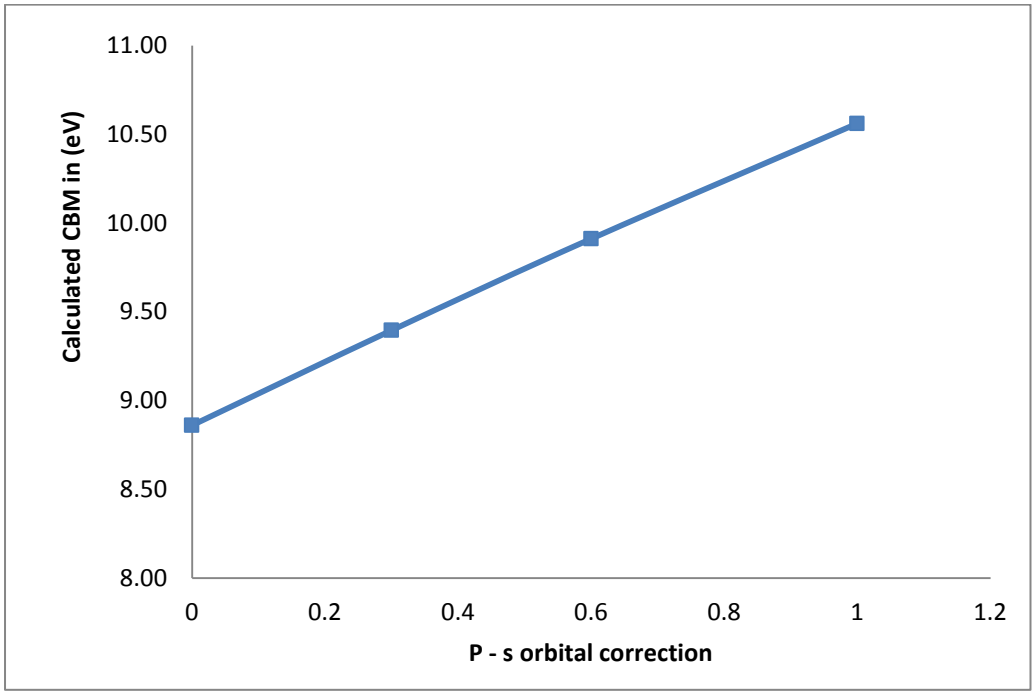

Figure 4.21 Plot between calculated *CBM* vs. P-p orbital correction of InP with In-s as 0.3

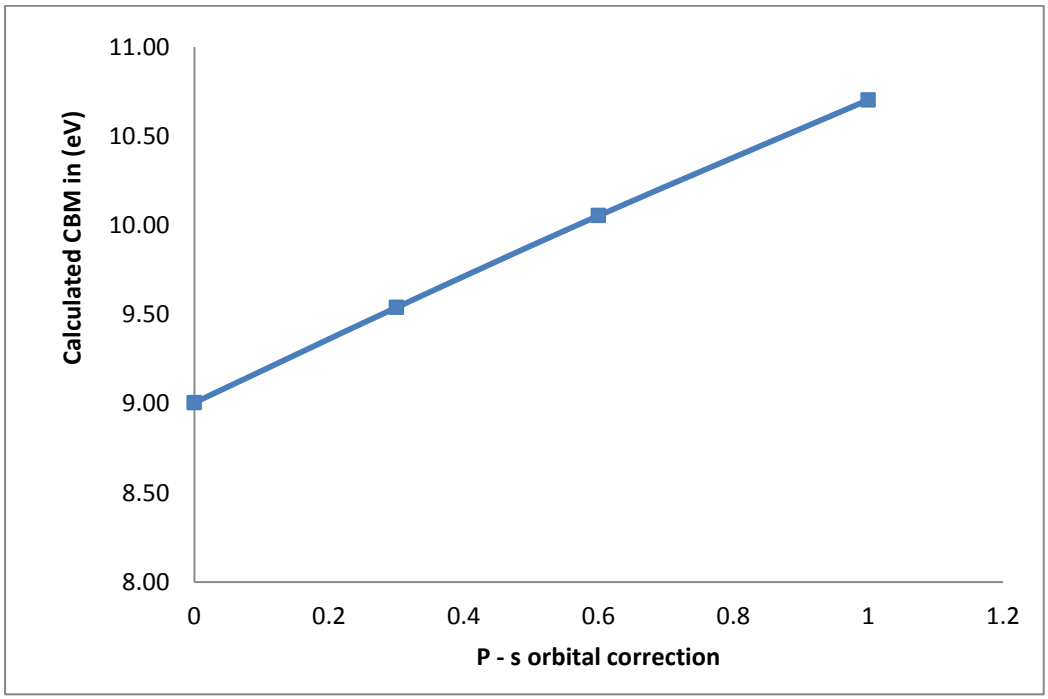

Figure 4.22 Plot between calculated *CBM* vs. P-p orbital correction of InP with In-s as 0.6

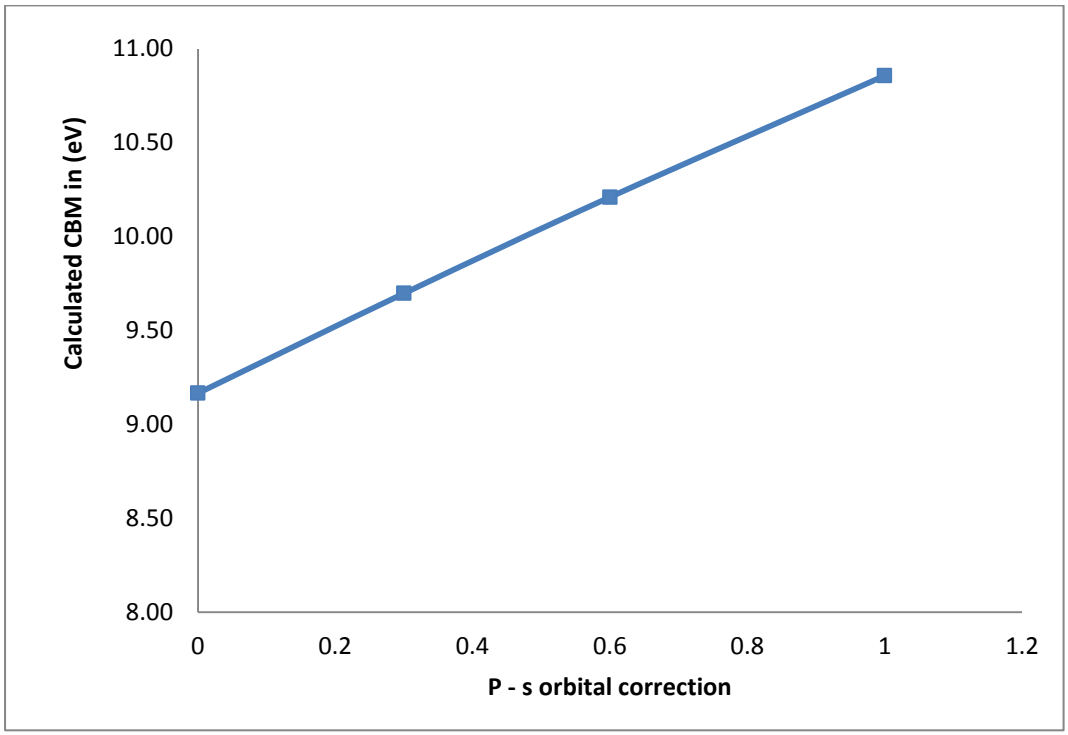

Figure 4.23 Plot between calculated *CBM* vs. P-p orbital correction of InP with In-s as 1.0

From the figure 4.20, it is clear that on changing the P-s orbital correction, *CBM* changes linearly. Similarly, plot between calculated *CBM* vs. P-s orbital correction of InP with In-Vs as 0.3 (figure 4.21), 0.6 (figure 4.22) and 1.0(figure 4.23) are linear.

Now, the value of P-s orbital correction at which the calculated *CBM* is same as the experimental *CBM*, as in table 4.2 is needed. A linear curve fitting of the P-s orbital correction vs. the difference between calculated *CBM* and target *CBM* is plotted for In-Vs correction value as 0.0 (figure 4.24) 0.3 (figure 4.25), 0.6 (figure 4.26) and 1.0(figure 4.27). As stated earlier in this chapter, since the relationship is linear, we can find the value of P-s orbital correction at which difference between calculated *CBM* and target

CBM is zero, which is nothing but the P-s orbital correction value when the calculated *CBM* is same as the target *CBM*.

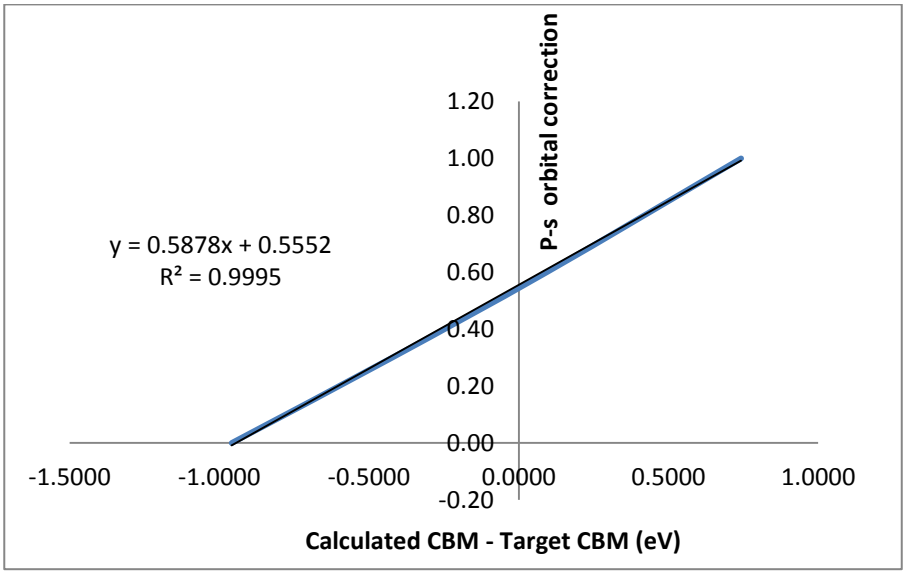

Figure 4.24 Plot between P-s orbital correction vs. the difference between calculated *CBM* and target *CBM* of InP with In-Vs as 0.0

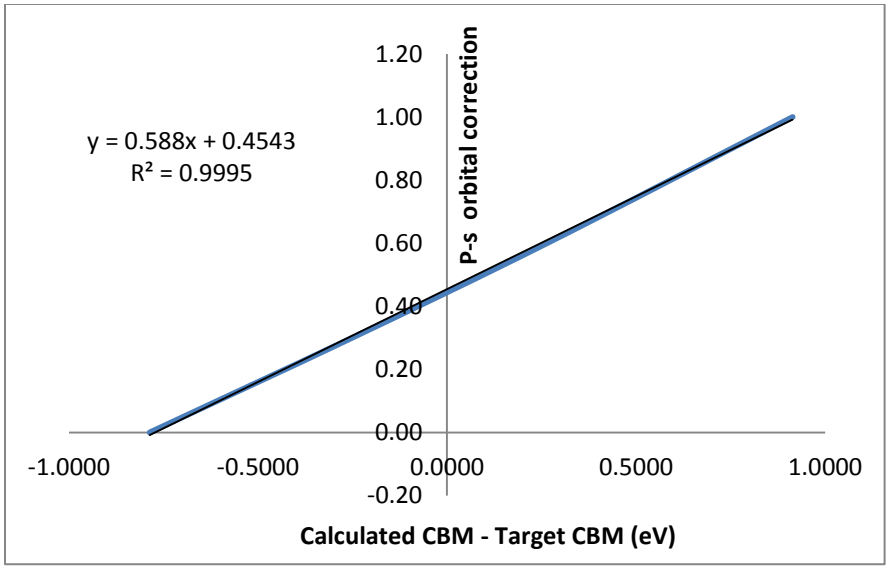

Figure 4.25 Plot between P-s orbital correction vs. the difference between calculated *CBM* and target *CBM* of InP with In-Vs as 0.3

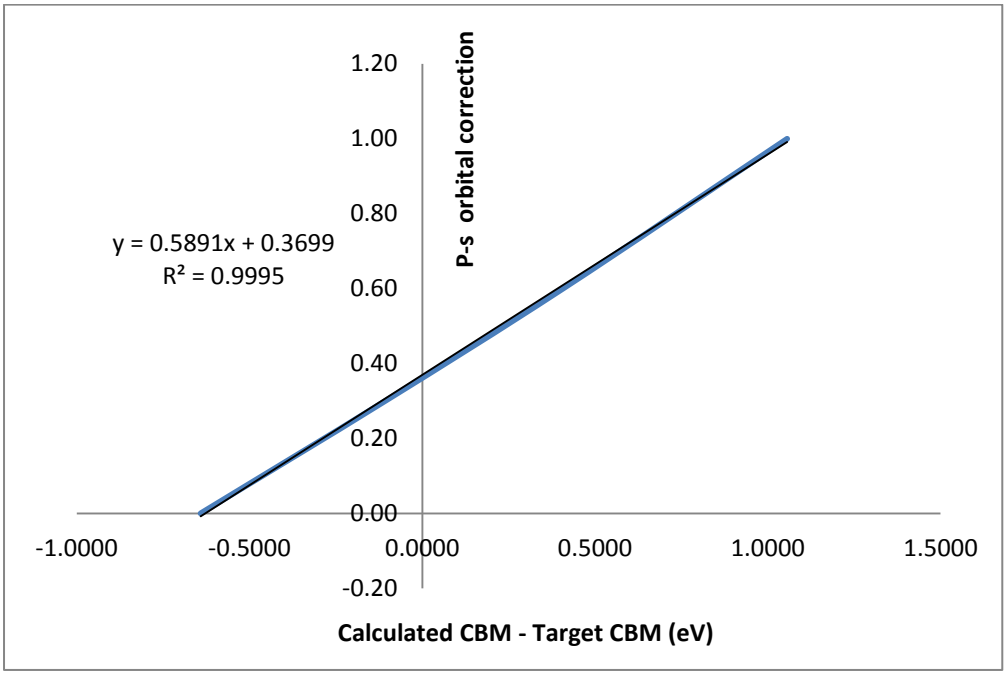

Figure 4.26 Plot between P-s orbital correction vs. the difference between calculated *CBM* and target *CBM* of InP with In-Vs as 0.6

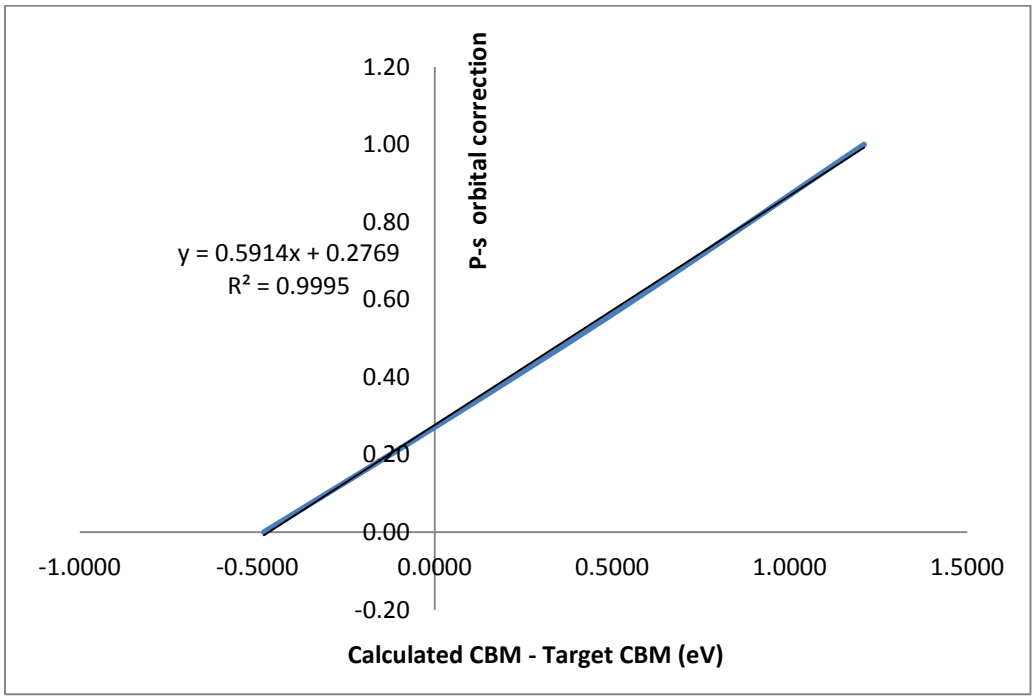

Figure 4.27 Plot between P-s orbital correction vs. the difference between calculated *CBM* and target *CBM* of InP with In-Vs as 1.0

Table 4.4 Summary of the P-s orbital fitted value for different In-s orbital values

In-s	**0.0**	**0.3**	**0.6**	**1.0**
P-s	0.5552	0.4543	0.3699	0.2769

The P-s orbital correction values from this step are summarized in the table 4.4. These values of P-p orbital correction will be used for further calculations. For the values of In-s and P-s correction in table 4.4 and other correction values from table 4.3, eigen energies are generated. Figure 4.28 is a plot between of difference between calculated *CBM, X_{1C}, X_{3C} and L_{1C}* and target *CBM, X_{1C}, X_{3C} and L_{1C}* vs. In-s orbital correction of InP. From the plot, it is clear that, when In-s orbital correction is 0.6 and P-s orbital correction is 0.3699, all the values are closer to zero, which indicates that the calculated *CBM, X_{1C}, X_{3C} and L_{1C}* values are closer to target *CBM, X_{1C}, X_{3C} and L_{1C}*.

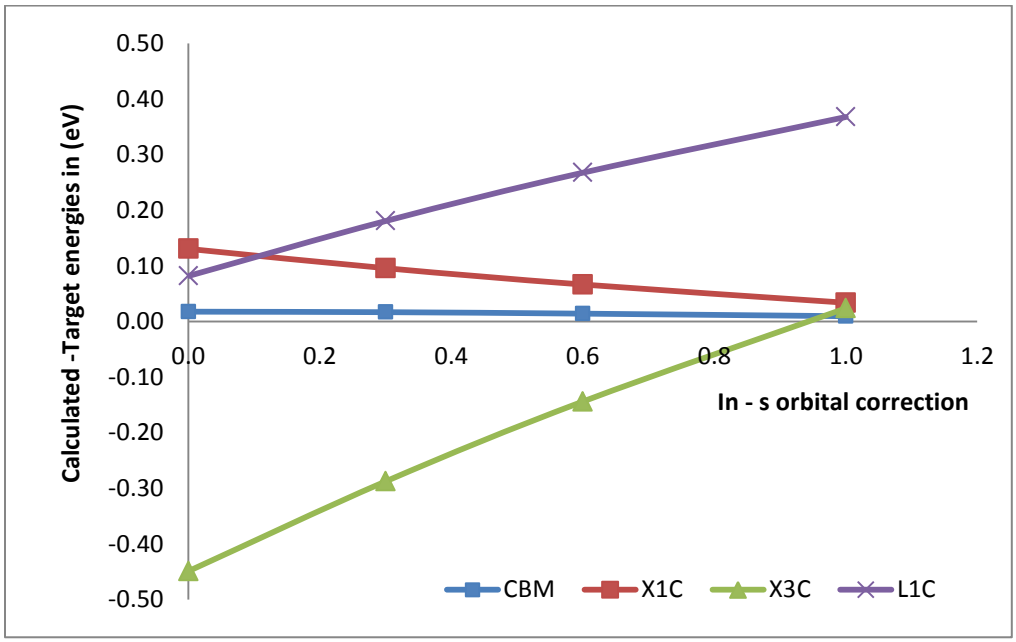

Figure 4.28 Plot between In-s orbital correction vs. the difference between calculated and target energies of InP

4.6.2. As-Fitting

For a In-s orbital correction value, As-s orbital correction value is changed and the energies at critical points are generated. Figure 4.29 is a plot between calculated *CBM* vs. As-s orbital correction of InAs with In-Vs as 0.0.

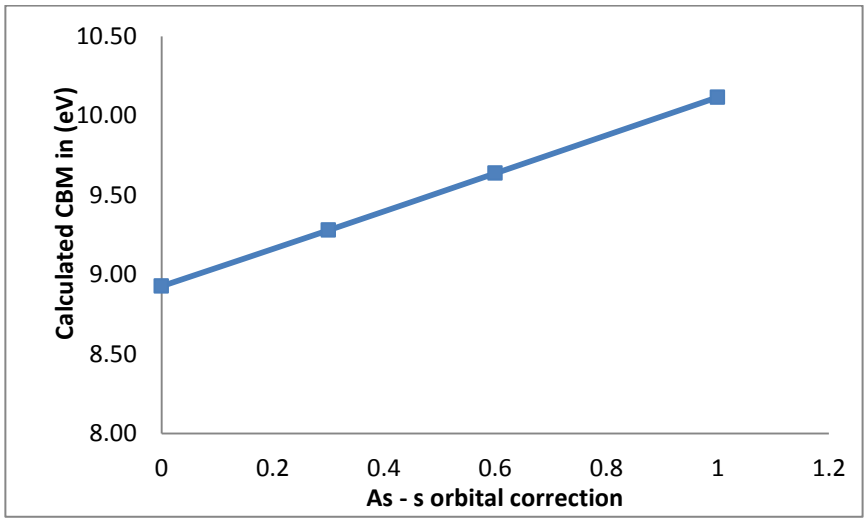

Figure 4.29 Plot between calculated *CBM* vs. As-p orbital correction of InAs with In-s as 0.0

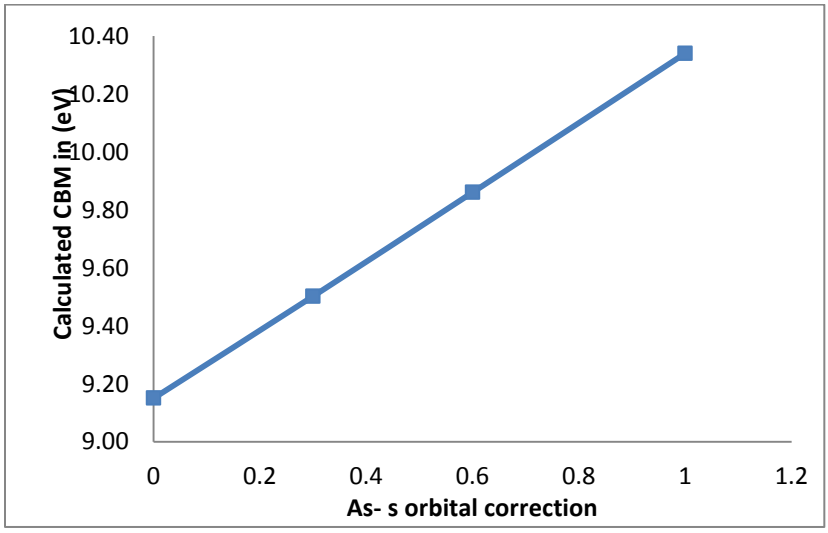

Figure 4.30 Plot between calculated *CBM* vs. As-p orbital correction of InAs with In-s as 0.3

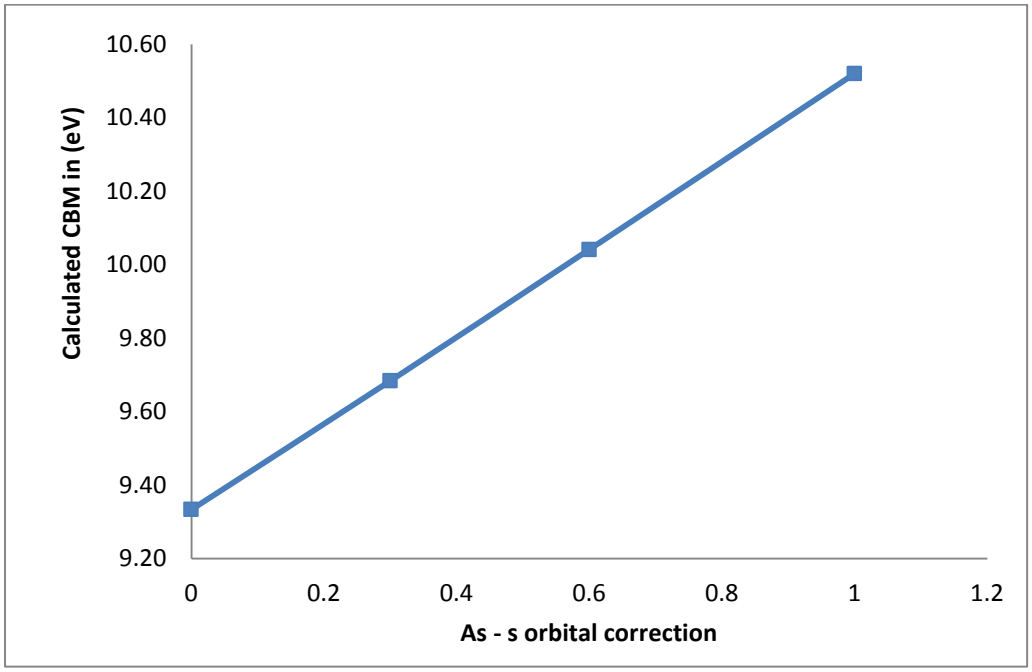

Figure 4.31 Plot between calculated *CBM* vs. As-p orbital correction of InAs with In-s as 0.6

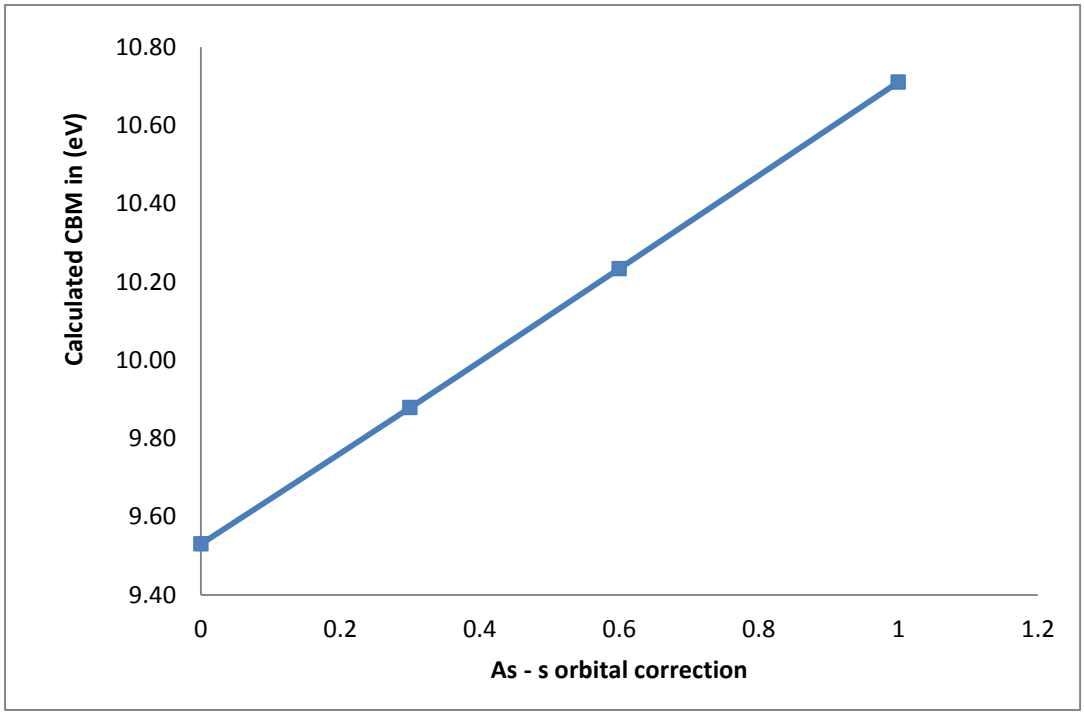

Figure 4.32 Plot between calculated *CBM* vs. As-p orbital correction of InAs with In-s as 1.0

From the figure 4.29, it is clear that on changing the As-s orbital correction, *CBM* changes linearly. Similarly, plot between calculated *CBM* vs. As-s orbital correction of InAs with In-Vs as 0.3 (figure 4.30), 0.6 (figure 4.31) and 1.0(figure 4.32) are linear.

Now, the value of As-s orbital correction at which the calculated *CBM* is same as the experimental *CBM*, as in table 4.2 is needed. A linear curve fitting of the As-s orbital correction vs. the difference between calculated *CBM* and target *CBM* is plotted for In-Vs correction value as 0.0 (figure 4.33) 0.3 (figure 4.34), 0.6 (figure 4.35) and 1.0(figure 4.36). As stated earlier in this chapter, since the relationship is linear, we can find the value of As-s orbital correction at which difference between calculated *CBM* and target *CBM* is zero, which is nothing but the As-s orbital correction value when the calculated *CBM* is same as the target *CBM*.

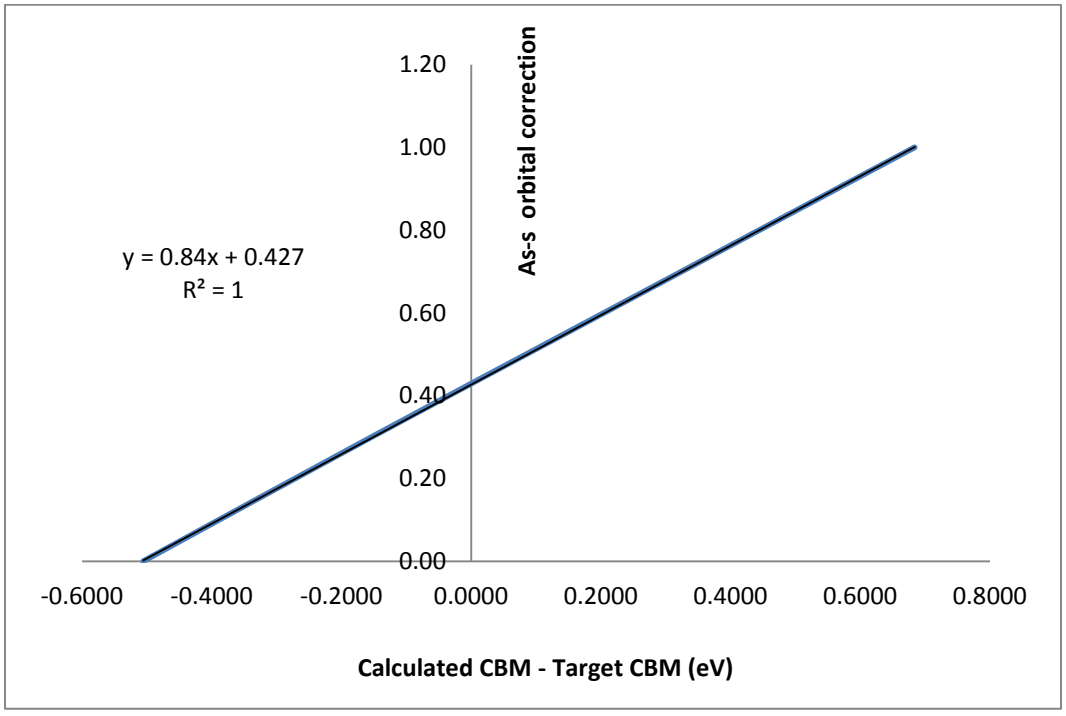

Figure 4.33 Plot between As-s orbital correction vs. the difference between calculated *CBM* and target *CBM* of InAs with In-Vs as 0.0

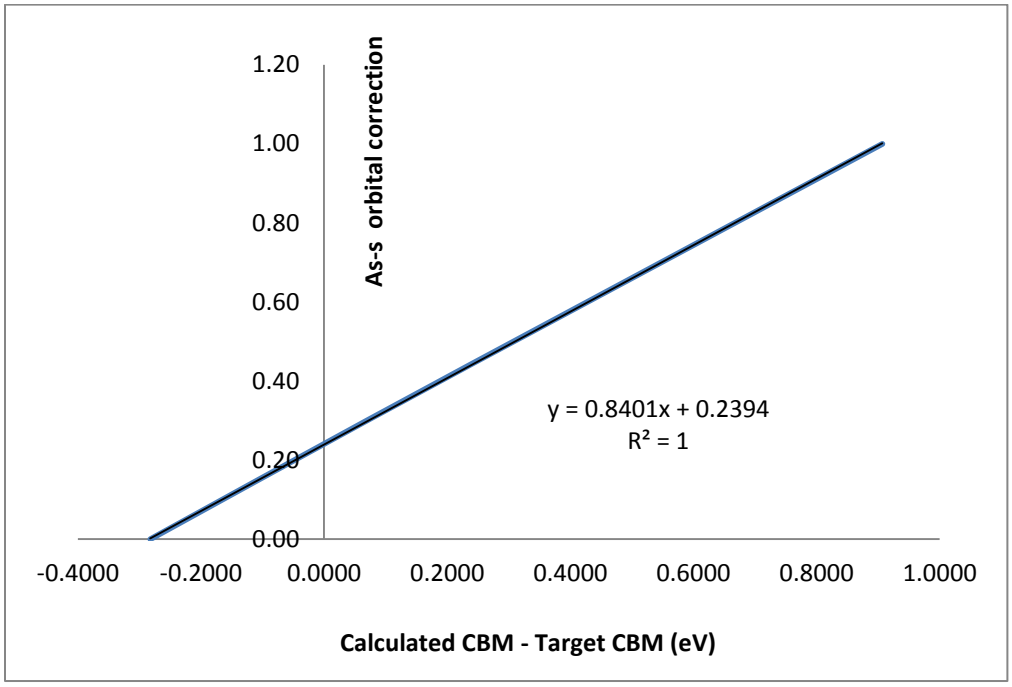

Figure 4.34 Plot between As-s orbital correction vs. the difference between calculated *CBM* and target *CBM* of InAs with In-Vs as 0.3

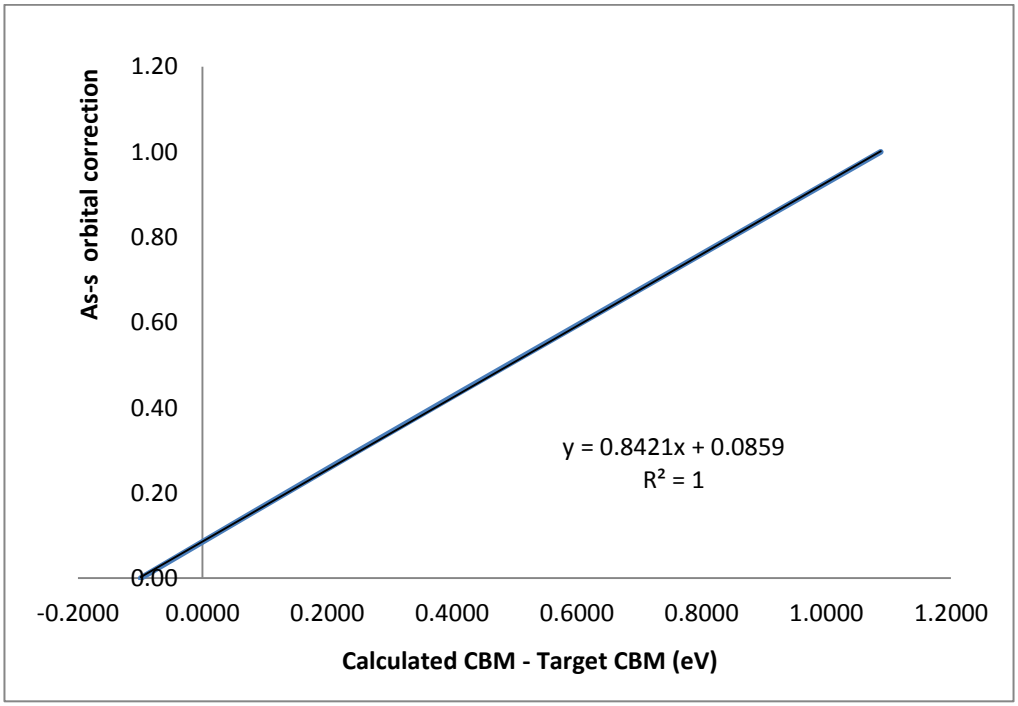

Figure 4.35 Plot between As-s orbital correction vs. the difference between calculated *CBM* and target *CBM* of InAs with In-Vs as 0.6

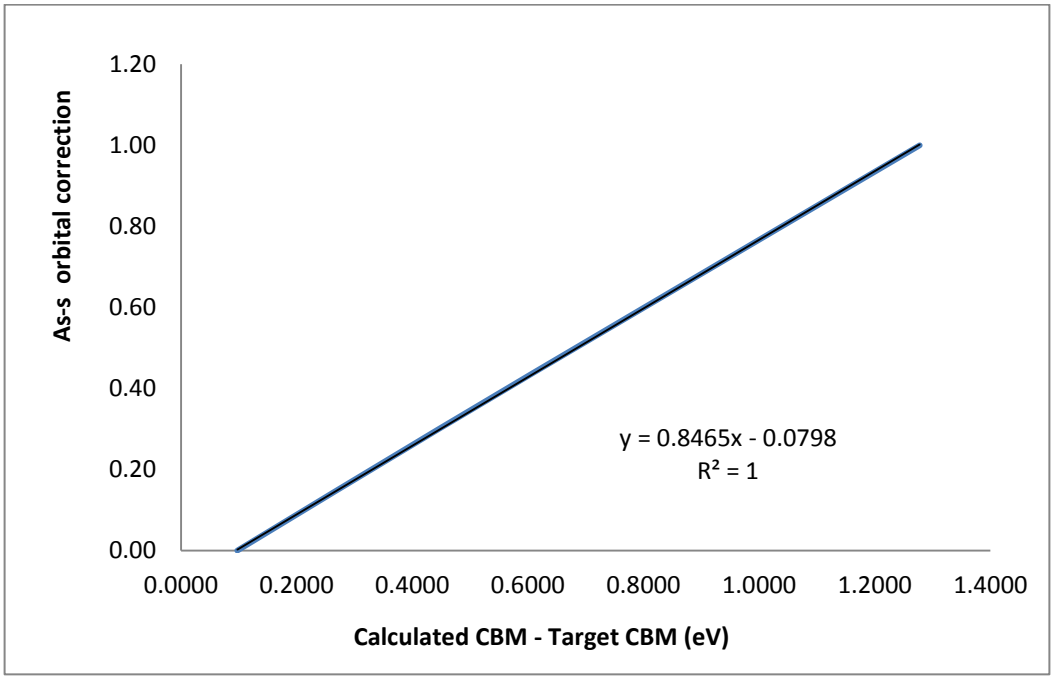

Figure 4.36 Plot between As-s orbital correction vs. the difference between calculated *CBM* and target *CBM* of InAs with In-Vs as 1.0

Table 4.5 Summary of the As-s orbital fitted value for different In-s orbital values

In-s	**0.0**	**0.3**	**0.6**	**1.0**
As-s	0.427	0.2394	0.0859	-0.0798

The As-s orbital correction values from this step are summarized in the table 4.5. These values of As-p orbital correction will be used for further calculations. For the values of In-s and As-s correction in table 4.5 and other correction values from table 4.2, eigen energies are generated. Figure 4.37 is a plot between of difference between calculated *CBM, X_{1C}, X_{3C} and L_{1C}* and target *CBM, X_{1C}, X_{3C} and L_{1C}* vs. In-s orbital correction of InAs. From the plot, it is clear that, when In-s orbital correction is 0.6 and As-s orbital correction is 0.0859, all the values are closer to zero, which indicates that the calculated *CBM, X_{1C}, X_{3C} and L_{1C}* values are closer to target *CBM, X_{1C}, X_{3C} and L_{1C}*.

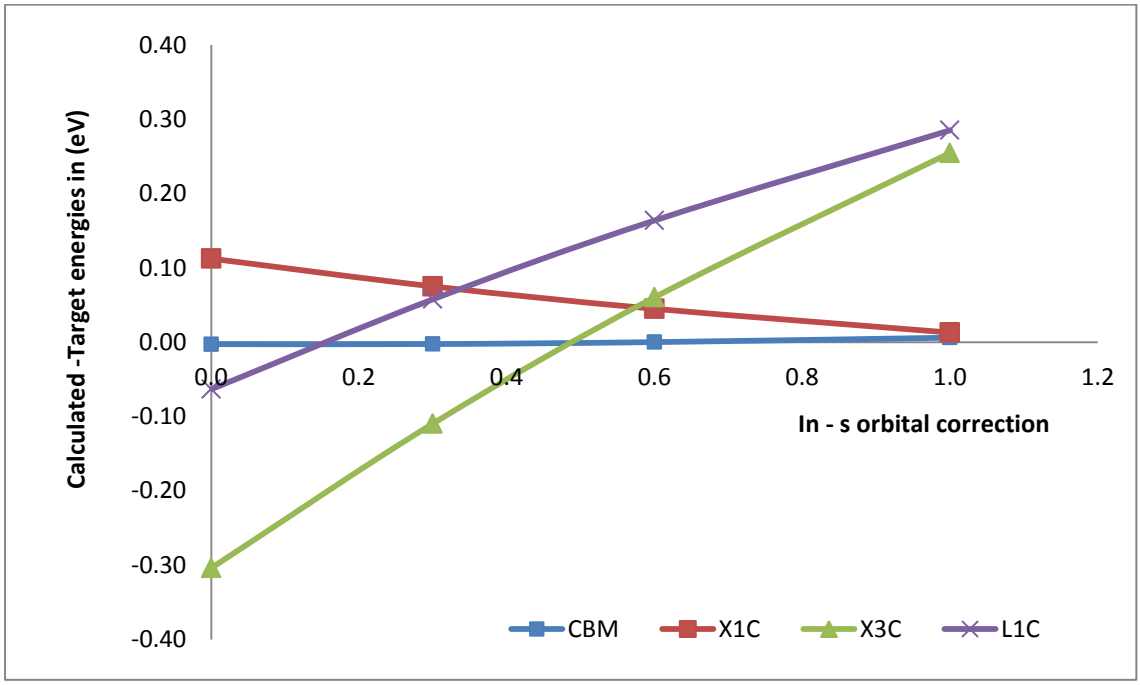

Figure 4.37 Plot between In-s orbital correction vs. the difference between calculated and target energies of InAs

4.6.3. Sb-Fitting

For a In-s orbital correction value, Sb-s orbital correction value is changed and the energies at critical points are generated. Figure 4.38 is a plot between calculated *CBM* vs. Sb-s orbital correction of InSb with In-Vs as 0.0.

From the figure 4.38, it is clear that on changing the Sb-s orbital correction, *CBM* changes linearly. Similarly, plot between calculated *CBM* vs. Sb-s orbital correction of InSb with In-Vs as 0.3 (figure 4.39), 0.6 (figure 4.40) and 1.0(figure 4.41) are linear.

Now, the value of Sb-s orbital correction at which the calculated CBM is same as the experimental CBM as in table 4.2 is needed. A linear curve fitting of the Sb-s orbital correction vs. the difference between calculated CBM and target CBM is plotted for In-

Vs correction value as 0.0 (figure 4.42) 0.3 (figure 4.43), 0.6 (figure 4.44) and 1.0(figure 4.45).

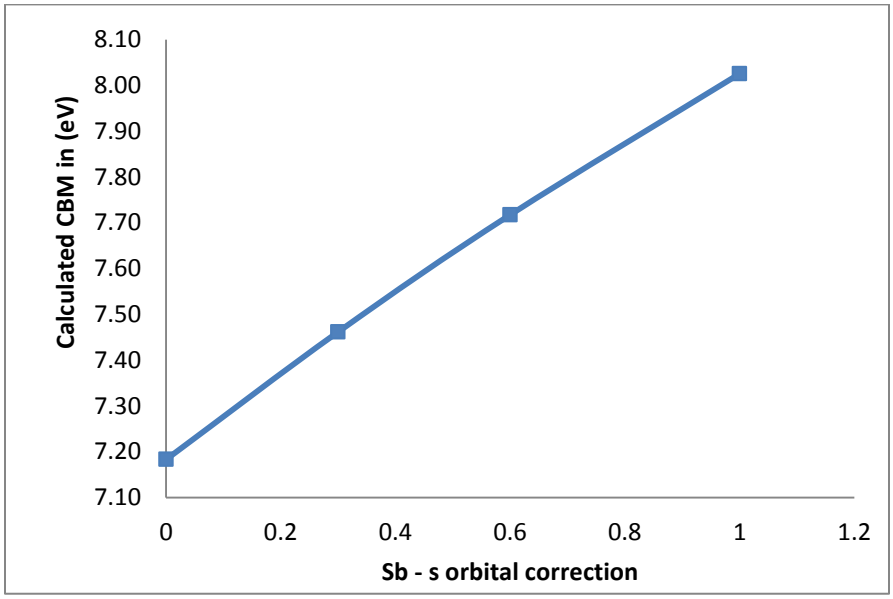

Figure 4.38 Plot between calculated *CBM* vs. Sb-p orbital correction of InSb with In-s as 0.0

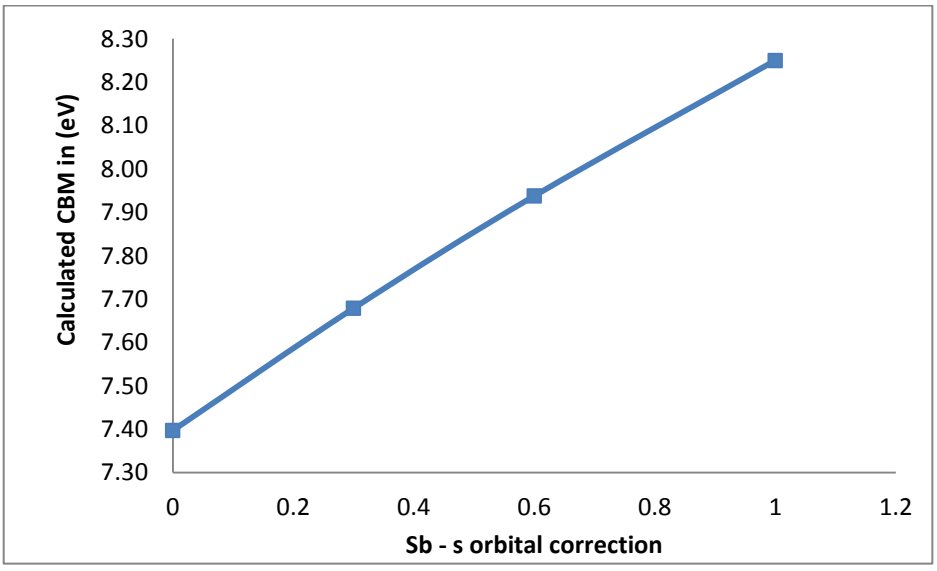

Figure 4.39 Plot between calculated *CBM* vs. Sb-p orbital correction of InSb with In-s as 0.3

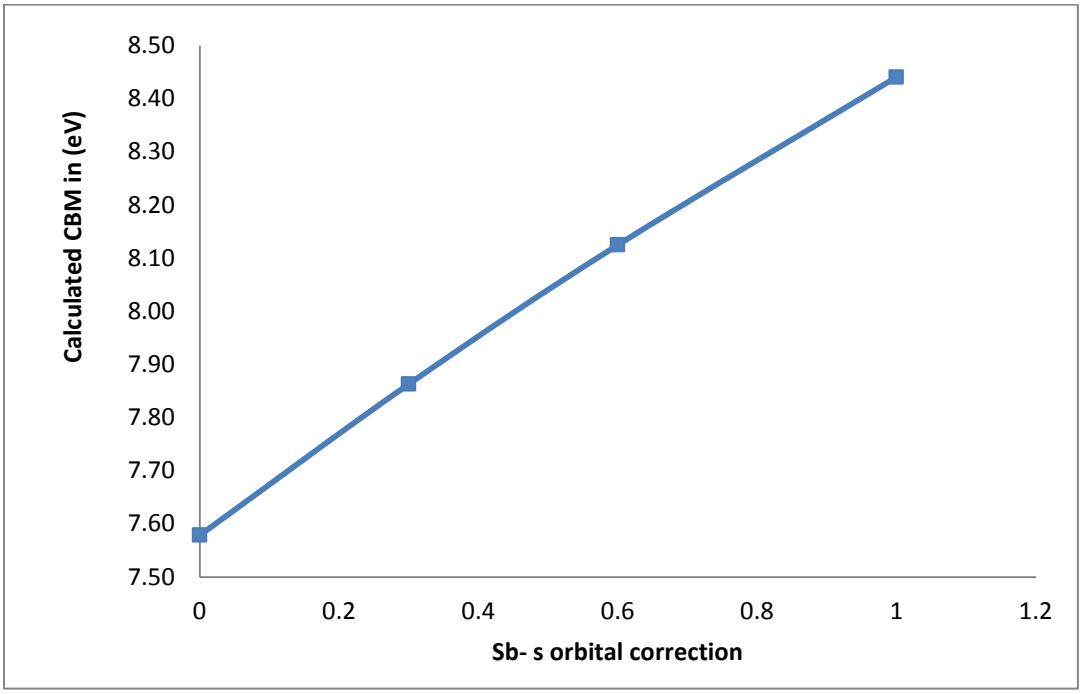

Figure 4.40 Plot between calculated *CBM* vs. Sb-p orbital correction of InSb with In-s as 0.6

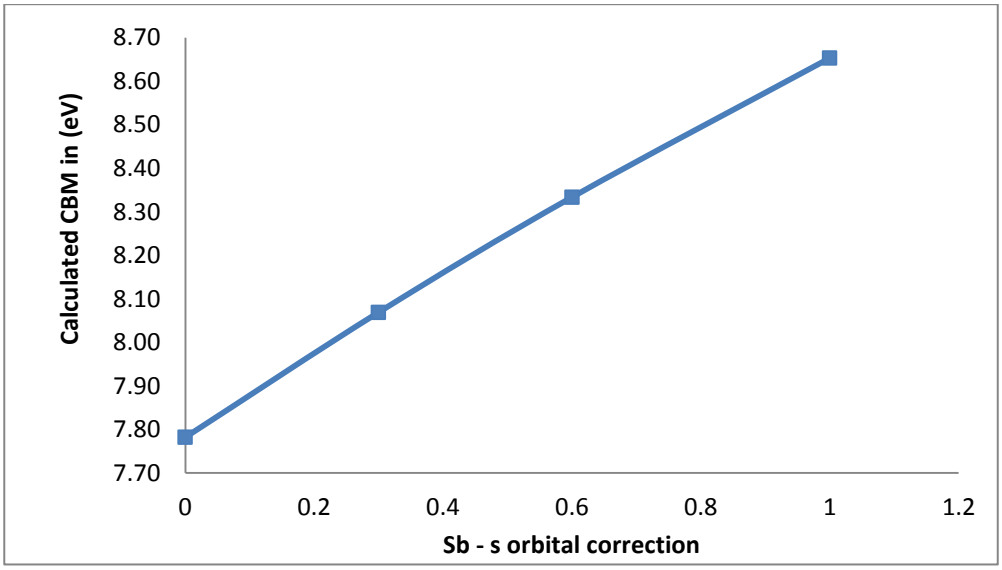

Figure 4.41 Plot between calculated *CBM* vs. Sb-p orbital correction of InSb with In-s as 1.0

As stated earlier in this chapter, since the relationship is linear, we can find the value of Sb-s orbital correction at which difference between calculated *CBM* and target *CBM* is zero, which is nothing but the Sb-s orbital correction value when the calculated *CBM* is same as the target *CBM*.

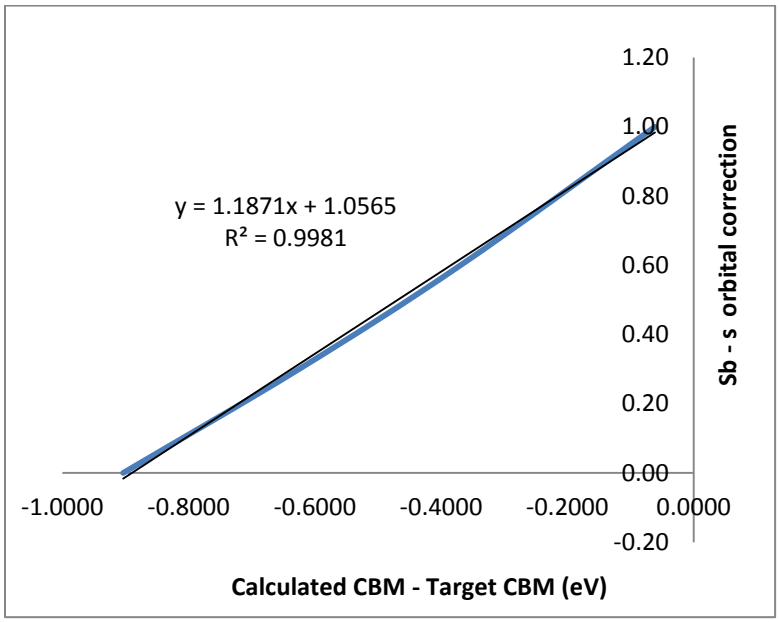

Figure 4.42 Plot between Sb-s orbital correction vs. the difference between calculated *CBM* and target *CBM* of InSb with In-Vs as 0.0

The Sb-s orbital correction values from this step are summarized in the table 4.6. These values of Sb-p orbital correction will be used for further calculations. For the values of In-s and Sb-s correction in table 4.6 and other correction values from table 4.2, eigen energies are generated.

Table 4.6 Summary of the Sb-s orbital fitted value for different In-s orbital values

In-s	**0.0**	**0.3**	**0.6**	**1.0**
As-s	1.0565	0.7929	0.5737	0.3345

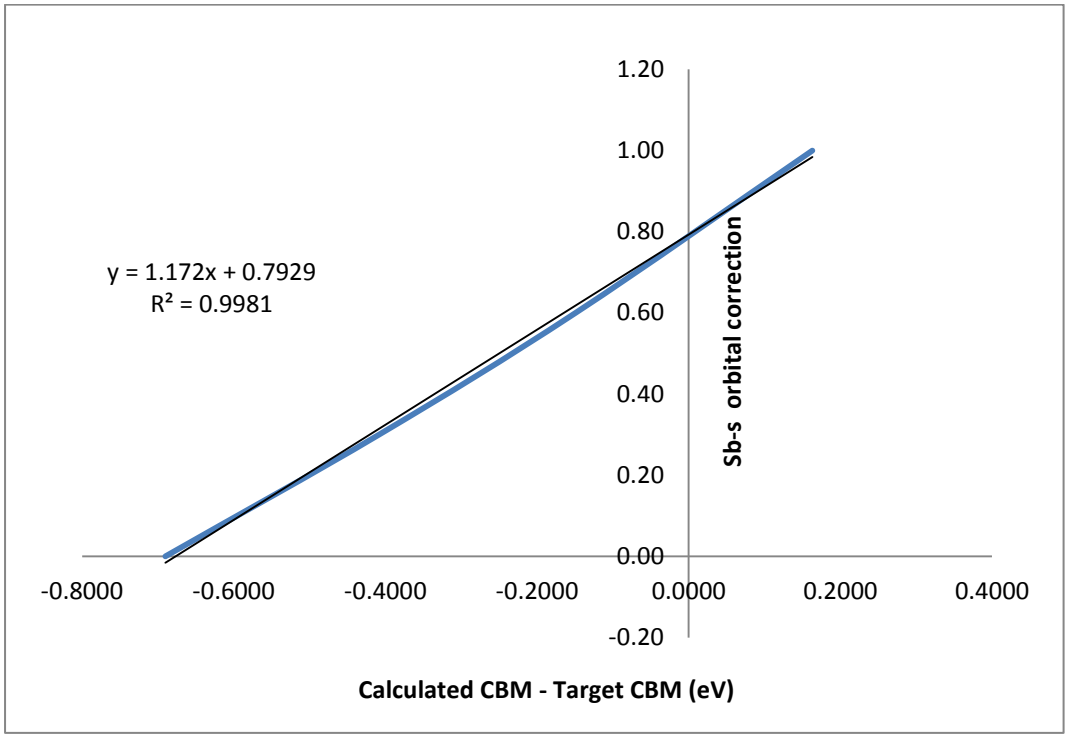

Figure 4.43 Plot between Sb-s orbital correction vs. the difference between calculated *CBM* and target *CBM* of InSb with In-Vs as 0.3

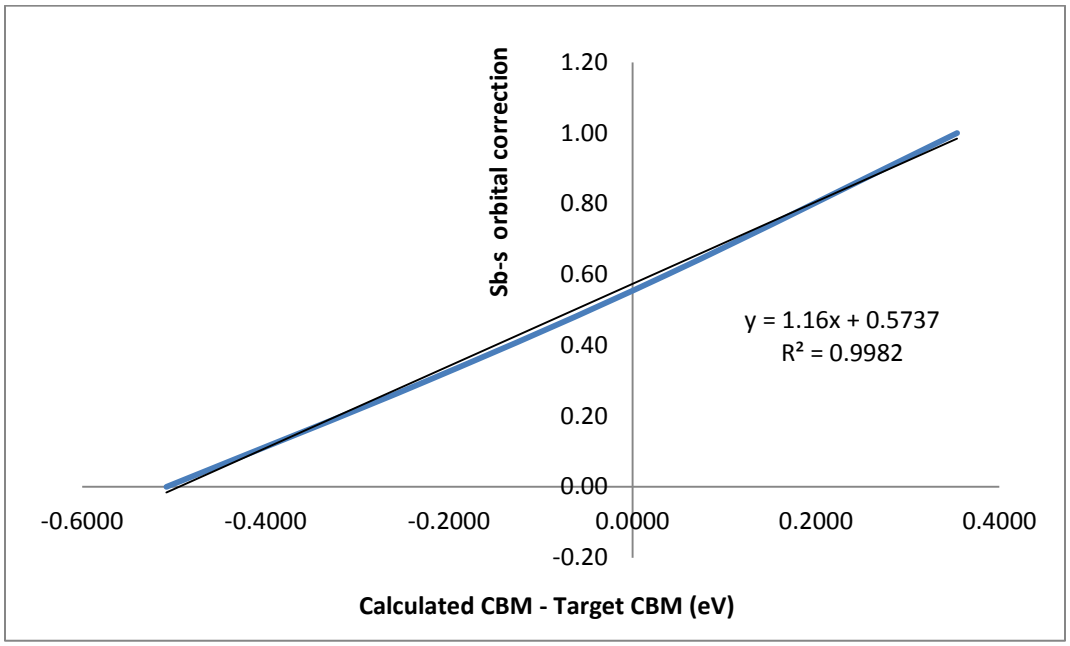

Figure 4.44 Plot between Sb-s orbital correction vs. the difference between calculated *CBM* and target *CBM* of InSb with In-Vs as 0.6

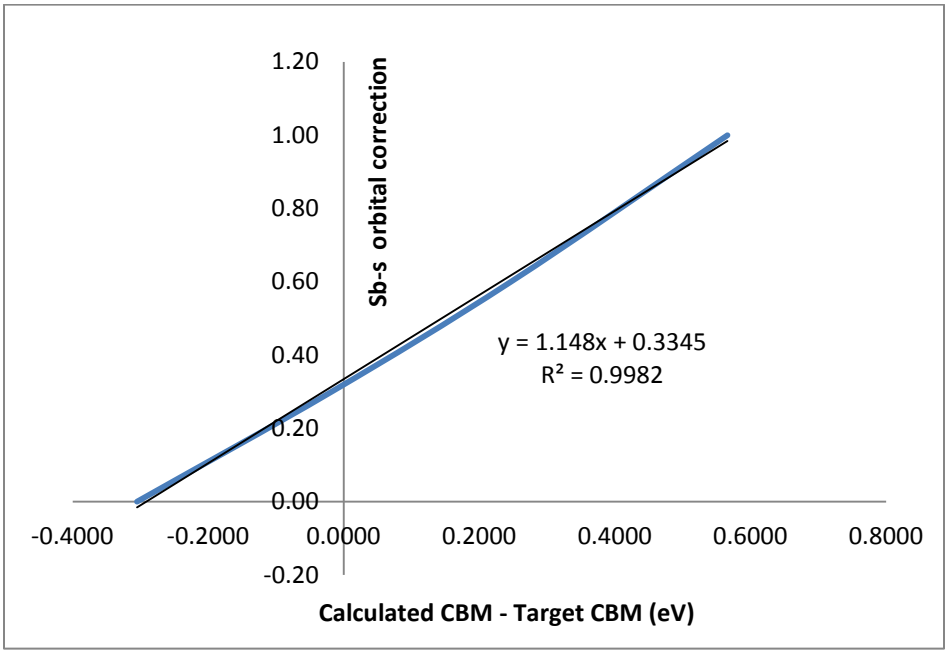

Figure 4.45 Plot between Sb-s orbital correction vs. the difference between calculated *CBM* and target *CBM* of InSb with In-Vs as 1.0

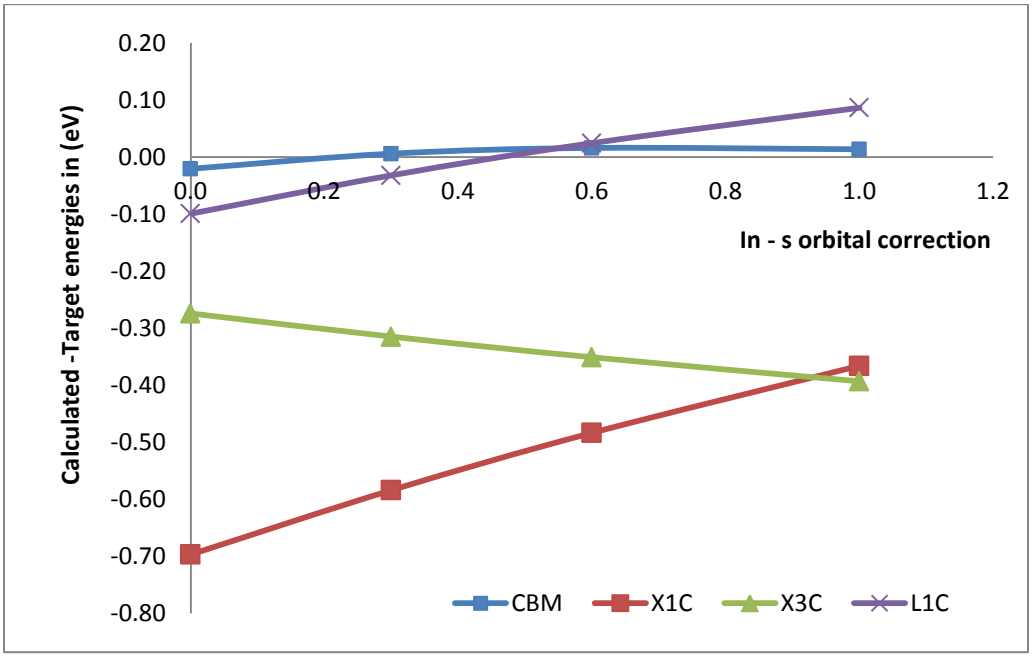

Figure 4.46 Plot between In-s orbital correction vs. the difference between calculated and target energies of InSb

Figure 4.46 is a plot between of difference between calculated *CBM, X_{1C}, X_{3C} and L_{1C}* and target *CBM, X_{1C}, X_{3C} and L_{1C}* vs. In-s orbital correction of InAs. From the plot, it is clear that, when In-s orbital correction is 0.6 and Sb-s orbital correction is 0.5737, all the values are closer to zero, which indicates that the calculated *CBM, X_{1C}, X_{3C} and L_{1C}* values are closer to target *CBM, X_{1C}, X_{3C} and L_{1C}*.

Table 4.7 Summary of the anion and cation, s, p and d orbital correction

	InP	**InAs**	**InSb**
In-d	-0.2779	-0.2779	-0.2779
In-p	8	8	8
In-s	0.6	0.6	0.6
V-d	8	8	8
V-p	-0.085	-0.0748	-0.3029
V-s	0.3699	0.0859	0.5737

The summary of fitting of s,p,d orbitals of cation (In) and anion (P, As, Sb) is given in table 4.7. These corrections will be used to elucidate the band structure of the bulk InV(V=P, As,Sb) semiconductors.

4.7. InV band error corrected DFT-LDA electronic structure

Using, the pseudopotential correction in the table 4.7, eigen energies at the critical points are calculated and tabulated in table 4.8.

From table 4.8, it is clear that the DFT-LDA calculated energies at critical points are fit to the experimental values in the order of less than 0.1 eV. The full band structure of InP, InAs, InSb is generated and plotted in figure 4.47, 4.48, 4.49 respectively. The plot also compares before and after atomic pseudopotential corrections. Solid lines are after fitting the pseudopotentials and dotted lines are before fitting the pseudopotentials.

Table 4.8 Energies at critical points in Brillouin zone. Theoretical energies are from DFT-LDA calculations after pseudopotential fitting. Energies are in eV

	InP		**InAs**		**InSb**	
	Target	Theory	Target	Theory	Target	Theory
Γ_{1C}	1.4236	1.4890	0.418	0.5479	0.2352	0.5163
X_{1C}	2.38	2.4977	2.01	2.1847	1.79	1.5716
X_{3C}	3.08	2.9873	2.50	2.6902	1.86	1.7741
L_{1C}	2.03	2.3488	1.55	1.8436	0.76	1.0495
E_{p-d}	16.8015	16.8585	17.0915	19.7908	17.2915	17.2516

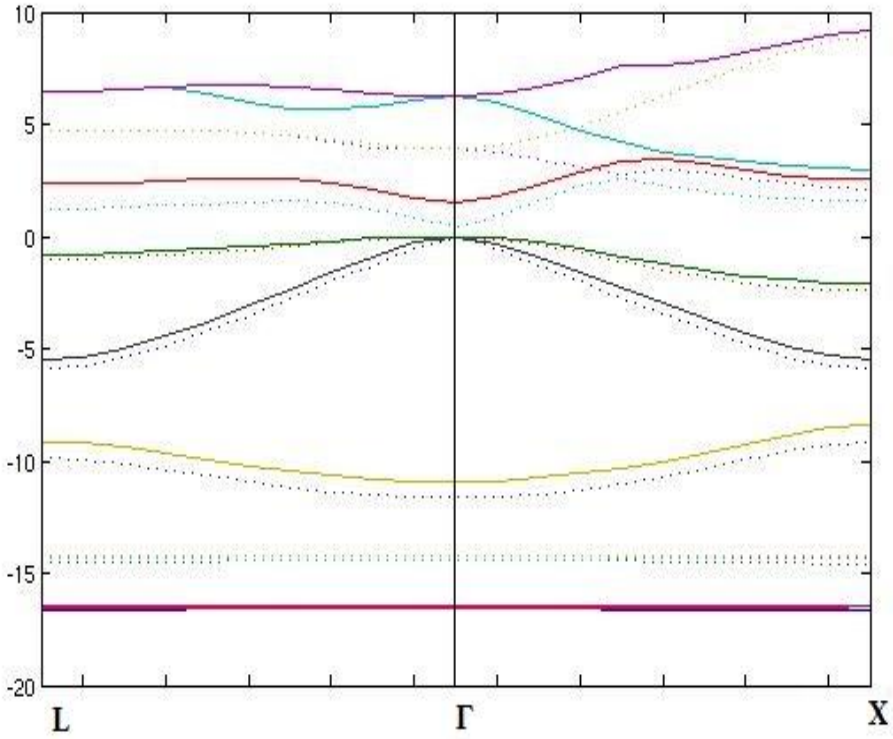

Figure 4.47 Band Structure of InP

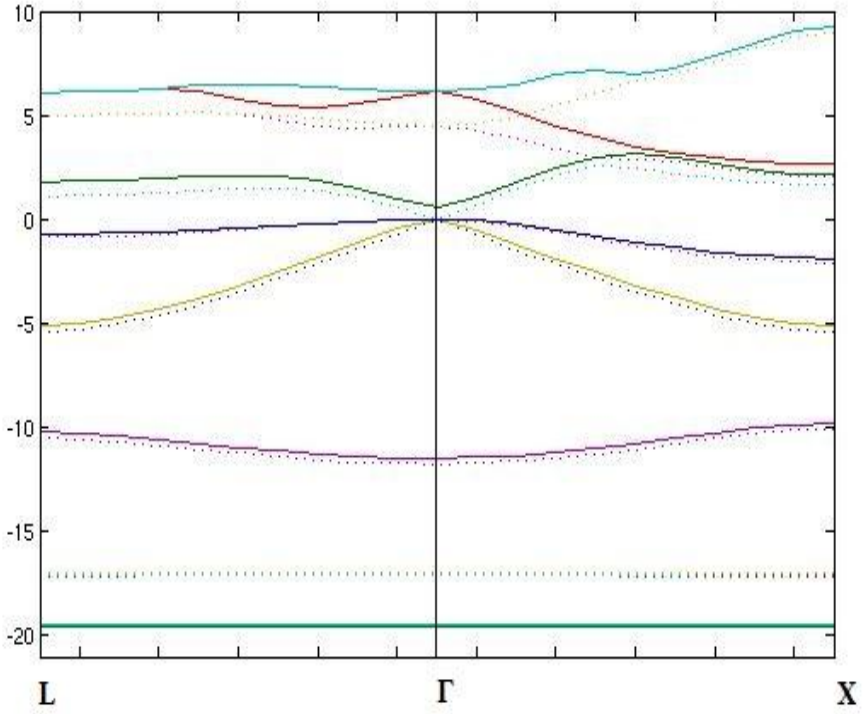

Figure 4.48 Band structure of InAs

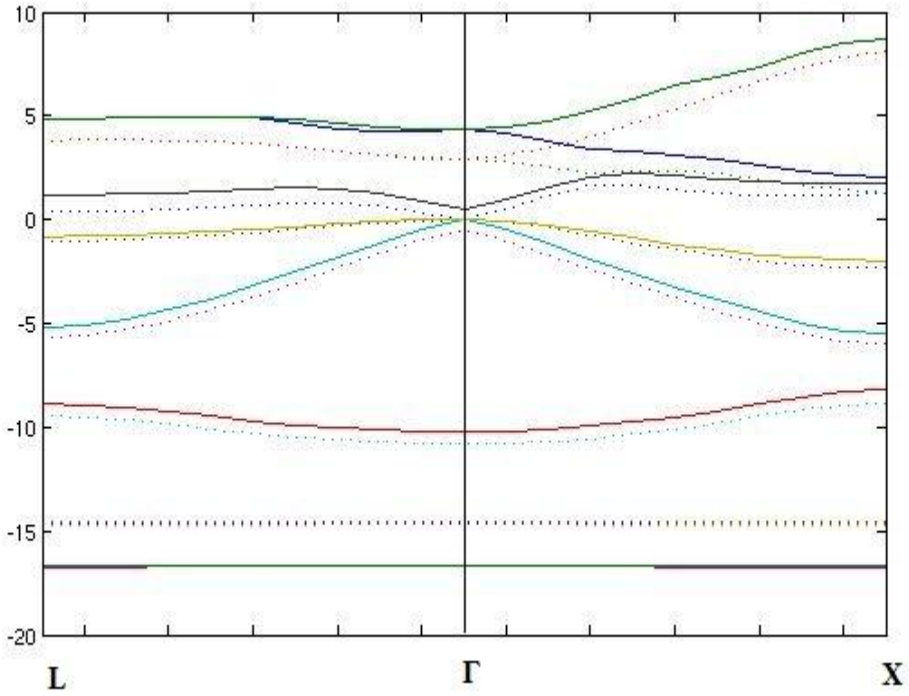

Figure 4.49 Band Structure of InSb

CHAPTER 5: CONCLUSION

In this work, we have applied a new empirical scheme to correct the electronic structures computed by DFT-LDA simultaneously for a set of binary semiconductors. We have calculated the electronic states of InP, InAs, and InSb by DFT-LDA calculation. The DFT-LDA bulk band structure has been corrected to yield the experimental band gaps at Γ, L, X points, and the experimentally measured separation of the valence bands derived from the p and d orbitals by modifying the nonlocal pseudopotentials.

The main conclusions can be summarized as follows.

a. The calculation provides an excellent evaluation of the scheme to correct the binary electronic structures generated by DFT-LDA calculations to the experimental results.
b. The band gap errors are corrected by adding corrections to the non-local part of the atomic orbital, after the self-consistent DFT-LDA calculation.
    i. d orbital of In is adjusted by fitting calculated $E_{p\text{-}d}$ to experimental $E_{p\text{-}d}$, producing the correct VBM level..
    ii. p orbital of In and d orbital of V (P, As, Sb) is adjusted by fitting calculated X_{1C} *and* X_{3C} to experimental X_{1C} *and* $X_{3C.}$
    iii. p orbital of V (P, As, Sb) is adjusted to keep the VBM level of step (i).

iv. s orbital of the cation (In) and anion V (V=P, As, Sb) is corrected by fitting calculated Γ_{1C} (CBM) and X_{1C}, X_{3C} and L_{1C} to experimental values.

c. Band gaps at critical points (Γ, L, X) calculated with the fitting results are in good agreement with the experimental results.

CHAPTER 6: FUTURE WORKS

This research work can be extended in several possible ways. Some of the suggestions are

a. The calculated correction factors can be compared to other binaries with similar anions like GaV (V=P, As, Sb, N) and AlV (V=P, As, Sb, N) semiconductors, and seek a common set of corrections for all III-V binaries.
b. Electronic structure of larger system like nano wires can be studied.
c. Band gap, optical absorption, and carrier localization of quantum heterostructures can also be studied.
d. Similar effort for group IV semiconductors, II-VI binaries, and the transferability to the mixed compounds of IV, III-V and II-VI.

REFERENCE

[1] "Basic Research Needs for Solar Energy Utilization," U.S. Department of Energy, U.S. Government Printing Office, Washington, DC, 2005.

[2] O. Mah, "Fundamentals of Photovoltaic Materials," National Solar Power Reasearch Institute, Inc., 1998.

[3] Y. Cui and S. Fan, "Manufacturable Nanostructured Solar Cells with Efficient Light Trapping and," Global Climate & Energy Project: Technical Report , 2012.

[4] M. B. Pelosi, "The Potential of III-V Semiconductors as Terrestrial Photovoltaic Devices," Progress in Photovoltaics: Research and Applications, vol. 15, pp. 51-68, 2007.

[5] O. D. Restrepo, R. Mishra and W. Windl, "First-principles study of InX (X=P,Sb) semiconductors," in American Physical Society March Meeting, 2012.

[6] S. Adolf Goetzberger, "Photovoltaic materials, history, status and outlook," Materials Science and Engineering R , vol. 40, pp. 1-46, 2003.

[7] B. Lax, "Experimental Investigations of Band Structure of Solids," Reviews of Modern Physics, vol. 30, p. 122, 1958.

[8] M. Cardona, Fundamentals of Semiconductors, Berlin: Springer-Verlag, 1999.

[9] Cohen, "Tight-Binding Calculations of the Valence Bands of Diamond and Zincblende Crystals," Phys. Stat. Sol. (b), vol. 68, p. 405, 1975.

[10] W. Kohn, "Motion of Electrons and Holes in Perturbed Periodic Fields," Phys. Rev, vol. 97, no. 4, p. 869, 1955.

[11] T. K. Bergstresser, "Band Structures and Pseudopotential Form Factors for Fourteen Semiconductors of the Diamond and Zinc-blende Structures," Phys. Rev, vol. 141, p. 789, 1966.

[12] M. L. Cohen, "Nonlocal pseudopotential calculations for the electronic structure of eleven diamond and zinc-blende semiconductors," Phys Rev. B, vol. 14, p. 556, 1976.

[13] L. W. Wang, "Large-scale local-density-approximation band gap-corrected GaAsN calculations," Applied Physics Letters, vol. 78, p. 1565, 2001.

[14] D. Vasileska, "Empirical Pseudopotential Method," nanohub, Tempe.

[15] K. P. Hohenberg, "Inhomogeneous electron gas," Physics Review B, vol. 136, p. 864, 1964.

[16] S. W. Kohn, "Self-consistent equations including exchange and correlation effects.," Physics Review , vol. 140, p. 1133, 1965.

[17] Yong Zhang, "Systematic approach to distinguishing a perturbed host state from an impurity state in a supercell calculation for a doped semiconductor: Using GaP:N as an example," Physical review B, vol. 74, p. 041201, 2006.

[18] Joshua Schrier, "Optical Properties of ZnO/ZnS and ZnO/ZnTe Heterostructures for Photovoltaic Applications," Nano Letters, vol. 7, no. 8, pp. 2377-2382, 2007.

[19] Gornik, "Proceeding of the 4th international Conference on the Physics of Narrow Gap Semiconductors," Springer-Verlag, Berlin, 1982.

[20] J. R. Chelikowsky, Solid State Communication, vol. 50, p. 105, 1984.

[21] I. Gorczyca, Physical Review B, vol. 39, p. 7705, 1989.

[22] E. Fortin, Physics Review B, vol. 12, p. 5803, 1975.

[23] S. Adachi, Physical Properties of III–V Semiconductor Compounds: InP, InAs, GaAs, GaP, InGaAs, and InGaAsP, Wiley, 1992.

[24] P. Bhattacharya, "Properties of Lattice-Matched and Strained Indium Gallium Arsenide," INSPEC, London, 1993.

[25] "Properties of Indium Phosphide," INSPEC: EMIS datareviews series, Newyork, 1991.

[26] Chow, IEEE Electron Device Letters, vol. 17, p. 69, 1996.

[27] J. R. M. et al, IEE Proceedings: Optoelectronics, vol. 145, p. 275, 1998.

[28] F. Matossi, Physical Review, vol. 111, p. 472, 1958.

[29] J. C. Woolley, Journal Physics, vol. 42, p. 1879, 1964.

[30] W. M. Coderre, Jounal Physics, vol. 46, p. 1207, 1968.

[31] Y. Lacroix, Journal of Applied Physics, vol. 80, p. 6416, 1996.

[32] O. Kane, J. Phys. Chem. Solids , vol. 1, p. 249, 1957.

[33] M. Razeghi, Opto-Electron. Review, vol. 6, p. 155, 1998.

[34] C. Kittel, Introduction to Solid State Physics, Newyork: Wiley, 1996.

[35] D. Leadley, "Semiconductors," Coventry, 2011.

[36] R. G. Parr, Density-Functional Theory of Atoms and Molecules, Oxford University Press, 1989.

[37] R. M. Dreizler, Density Functional Theory, 1990: Springer.

[38] C. Payne, "Gradients, Iterative minimization techniques for ab initio total-energy calculations: molecular dynamics and conjugate," Review Modern Physics, vol. 64, p. 1045, 1992.

[39] C. Payne, "Iterative minimization techniques for ab initio total-energy calculations: molecular dynamics and conjugate gradients," Review Modern Physics, vol. 64, p. 1045, 1992.

[40] Svane, "Quasiparticle self-consistent GW theory of III-V nitride semiconductors: Bands, gap bowing, and effective masses," Physics Review B, vol. 82, p. 115102, 2010.

[41] D. Vanderbilt, " Soft self-consistent pseudopotentials in a generalized eigen-value formalism," Physics Review B , vol. 41, p. 7892, 1990.

[42] Y. Zhang, "Effects of heavy nitrogen doping in III–V semiconductors – How well does the conventional wisdom hold for the dilute nitrogen “III–V-N alloys”?," Physica Status Solidi B , vol. 240, p. 396, 2003.

[43] Y. Zhang, "Similar and dissimilar aspects of III-V semiconductors containing Bi versus N," Physical Review B, vol. 71, p. 155201, 2005.

[44] L. W. Wang, " Planewave total energy code (PEtot)," NERSC, 2010. [Online]. Available: https://hpcrd.lbl.gov/~linwang/PEtot/PEtot.html. [Accessed 2012].

[45] L. Ley, "Total valence-band densities of states of III-V and II-VI compounds from x-ray photoemission spectroscopy," Physics Review B, vol. 9, p. 600, 1974.

[46] J.P. Perdew, Physics Review B, vol. 23, p. 5048, 1984.

[47] D.M. Ceperley, Physics Review Letters, vol. 45, p. 566, 1980.

[48] K. T. Haruna K, Journal of Physics C: Solid State Physics, vol. 20, p. 5275, 1987.

[49] A. G. Ozolinsh J.V, Soviet Physics Crystallography, vol. 7, p. 691, 1963.

[50] R.B, Journal of Physical Chemistry: Solids, vol. 26, p. 803, 1965.

[51] S. G. Xuejun Zhu, "Quasiparticle band structure of thirteen semiconductors and insulators," Physical Review B, vol. 43, no. 17, p. 142, 1991.

[52] Yoon-Suk Kim, "Accurate band structures and effective masses for InP, InAs, and InSb using hybrid functionals," Physical Review B, vol. 80, p. 035203, 2009.

[53] Y. Zhang, "Impurity perturbation to the host band structure and recoil of the impurity state," Physical Review B, vol. 68, p. 075210, 2003.

[54] L Ley, "Total valence-band densities of states of III-V and II-VI compounds from x-ray photoemission spectroscopy," Physical Review B, vol. 9, 1974.

APPENDIX A. SAMPLE KPT.INPUT FILE OF InP

```
-------------------------------------------------------------
xatom.InP                     |the name of atom.config file
10.05466                      |a0
8.0     0.      0.      1     |real space v(:,1), and kshif(1)
0.0     8.0     0.      1     |real space v(:,2), and kshif(2)
0.0     0.0     8.0     1     |real space v(:,3), and kshif(3)
-------------------------------------------------------------
```

APPENDIX B. SAMPLE ATOM.CONFIG FILE OF InP

```
2                                   | natom
5.54233    5.54233   0.00000      | AL(1,1), AL(2,1), AL(3,1) (a.u)
5.54233    0.0       5.54233      | AL(1,2), AL(2,2), AL(3,2)
0.0        5.54233   5.54233      | AL(1,3), AL(2,3), AL(3,3)

15 0.0   0.0   0.0   0  0  0      | iatom, x1,x2,x3, im1,im2,im3
49 0.25  0.25  0.25  0  0  0
*************************************************************
```